doi:10.1093/brain/awr348 Brain 2012: 135; 833–846 | 833

BRAIN
A JOURNAL OF NEUROLOGY

Non-human primate model of amyotrophic lateral sclerosis with cytoplasmic mislocalization of TDP-43

Azusa Uchida,[1] Hiroki Sasaguri,[1] Nobuyuki Kimura,[2] Mio Tajiri,[1] Takuya Ohkubo,[1] Fumiko Ono,[3] Fumika Sakaue,[1] Kazuaki Kanai,[4] Takashi Hirai,[5] Tatsuhiko Sano,[1] Kazumoto Shibuya,[4] Masaki Kobayashi,[1] Mariko Yamamoto,[1] Shigefumi Yokota,[1] Takayuki Kubodera,[1] Masaki Tomori,[5] Kyohei Sakaki,[5] Mitsuhiro Enomoto,[5] Yukihiko Hirai,[6] Jiro Kumagai,[7] Yasuhiro Yasutomi,[2] Hideki Mochizuki,[8] Satoshi Kuwabara,[4] Toshiki Uchihara,[9] Hidehiro Mizusawa[1] and Takanori Yokota[1]

1 Department of Neurology and Neurological Science, Graduate School of Medicine, Tokyo Medical and Dental University, Tokyo 113-8519, Japan
2 Tsukuba Primate Research Centre, National Institute of Biomedical Innovation, Tsukuba 305-0843, Japan
3 Corporation for Production and Research of Laboratory Primates, Tsukuba 305-0843, Japan
4 Department of Neurology, Graduate School of Medicine, Chiba University, Chiba 260-8670, Japan
5 Department of Orthopaedic Surgery, Graduate School of Medicine, Tokyo Medical and Dental University, Tokyo 113-8519, Japan
6 Department of Biochemistry and Molecular Biology, Nippon Medical School, Tokyo 113-8602, Japan
7 Department of Pathology, Graduate School of Medicine, Tokyo Medical and Dental University, Tokyo 113-8519, Japan
8 Department of Neurology, Kitasato University School of Medicine, Kanagawa 228-8555, Japan
9 Laboratory of Structural Neuropathology, Tokyo Metropolitan Institute of Medical Science, Tokyo 156-8506, Japan

Correspondence to: Takanori Yokota,
Department of Neurology and Neurological Science,
Graduate School of Medicine,
Tokyo Medical and Dental University,
Bunkyo-ku, Tokyo 113-8519,
Japan
E-mail: tak-yokota.nuro@tmd.ac.jp

Amyotrophic lateral sclerosis is a fatal neurodegenerative disease characterized by progressive motoneuron loss. Redistribution of transactive response deoxyribonucleic acid-binding protein 43 from the nucleus to the cytoplasm and the presence of cystatin C-positive Bunina bodies are considered pathological hallmarks of amyotrophic lateral sclerosis, but their significance has not been fully elucidated. Since all reported rodent transgenic models using wild-type transactive response deoxyribonucleic acid-binding protein 43 failed to recapitulate these features, we expected a species difference and aimed to make a non-human primate model of amyotrophic lateral sclerosis. We overexpressed wild-type human transactive response deoxyribonucleic acid-binding protein 43 in spinal cords of cynomolgus monkeys and rats by injecting adeno-associated virus vector into the cervical cord, and examined the phenotype using behavioural, electrophysiological, neuropathological and biochemical analyses. These monkeys developed progressive motor weakness and muscle atrophy with fasciculation in distal hand muscles first. They also showed regional cytoplasmic transactive response deoxyribonucleic acid-binding protein 43 mislocalization with loss of nuclear transactive response deoxyribonucleic acid-binding protein 43 staining in the lateral nuclear group of spinal cord innervating distal hand muscles and cystatin C-positive cytoplasmic aggregates, reminiscent of the spinal cord pathology of patients with amyotrophic lateral sclerosis. Transactive response deoxyribonucleic acid-binding protein 43 mislocalization was

Received July 27, 2011. Revised October 26, 2011. Accepted November 14, 2011. Advance Access publication January 17, 2012

an early or presymptomatic event and was later associated with neuron loss. These findings suggest that the transactive response deoxyribonucleic acid-binding protein 43 mislocalization leads to α-motoneuron degeneration. Furthermore, truncation of transactive response deoxyribonucleic acid-binding protein 43 was not a prerequisite for motoneuronal degeneration, and phosphorylation of transactive response deoxyribonucleic acid-binding protein 43 occurred after degeneration had begun. In contrast, similarly prepared rat models expressed transactive response deoxyribonucleic acid-binding protein 43 only in the nucleus of motoneurons. There is thus a species difference in transactive response deoxyribonucleic acid-binding protein 43 pathology, and our monkey model recapitulates amyotrophic lateral sclerosis pathology to a greater extent than rodent models, providing a valuable tool for studying the pathogenesis of sporadic amyotrophic lateral sclerosis.

Keywords: TDP-43; Bunina bodies; cystatin C; cynomolgus monkeys; amyotrophic lateral sclerosis

Abbreviations: AAV = adeno-associated virus; ALS = amyotrophic lateral sclerosis; FTLD = frontotemporal lobar degeneration; HEK = human embryonic kidney; TDP-43 = transactive response DNA-binding protein 43

Introduction

Amyotrophic lateral sclerosis (ALS), also known as Lou Gehrig's disease, is an incurable progressive neurodegenerative disease characterized by muscle weakness and atrophy resulting from the combined loss of upper and lower motoneurons. Most cases of ALS are sporadic, and only 10% of ALS cases are of a familial form. Protein aggregates are one histopathological characteristic of ALS. A breakthrough in understanding ALS pathogenesis was the discovery of the 43-kDa transactive response DNA-binding protein (TDP-43), which was recently identified as the major component of the protein aggregates and of the insoluble fraction in the brains of patients with sporadic ALS and frontotemporal lobar degeneration (FTLD) (Arai *et al.*, 2006; Neumann *et al.*, 2006). TDP-43 is now expected to play an essential role in the pathogenesis of sporadic ALS, possibly equivalent to that of tau and beta amyloid in Alzheimer's disease or α-synuclein in Parkinson's disease.

Human TDP-43 is a highly conserved and ubiquitously expressed 414 amino acid nuclear protein that binds to both DNA and RNA (Ou *et al.*, 1995; Buratti *et al.*, 2001). In normal settings, TDP-43 is a primarily nuclear protein that functions in transcription regulation, alternative splicing and RNA stabilization (Buratti *et al.*, 2008), as well as in microRNA metabolism (Buratti *et al.*, 2010). Pathological TDP-43 can be abnormally truncated, phosphorylated and ubiquitinated, and most TDP-43 is mislocalized from the nucleus to the cytoplasm or neurites (Arai *et al.*, 2006; Neumann *et al.*, 2006). Of note, almost all neurons with cytoplasmic TDP-43 accumulations show a dramatic depletion of normal nuclear TDP-43. Thus, both gain and loss of functions are potential disease mechanisms, either due to the loss of normal nuclear TDP-43 expression, or cytoplasmic mislocalization (Arai *et al.*, 2006; Neumann *et al.*, 2006; Cairns *et al.*, 2007). Therefore, cytoplasmic TDP-43 mislocalization with loss of its nuclear staining is a key feature found in the majority of patients' brains and spinal cords (Arai *et al.*, 2006; Neumann *et al.*, 2006).

TDP-43 strictly regulates its messenger RNA levels by directly binding to an intron in the 3′-untranslated region of its own transcript and enhancing its splicing (Ayala *et al.*, 2010; Polymenidou *et al.*, 2011), however, the expression level of TDP-43 can be upregulated ~1.5-fold (Mishra *et al.*, 2007; Gitcho *et al.*, 2009) in FTLD/ALS. Moreover, mutations in the *TDP-43* gene are associated with familial ALS (Kabashi *et al.*, 2008; Yokoseki *et al.*, 2008), in which TDP-43 is also frequently mislocalized within motoneurons of the spinal cord. These reports support the hypothesis that mislocalization of this protein plays a central role in the disease pathogenesis. The rodent, *Drosophila*, *Ceanorhabditis elegans* and zebrafish models with overexpressed mutant as well as wild-type TDP-43 show severe motor symptoms and wild-type TDP-43 localizes exclusively or primarily to nuclei (Ash *et al.*, 2010; Hanson *et al.*, 2010; Kabashi *et al.*, 2010; Li *et al.*, 2010; Shan *et al.*, 2010; Voigt *et al.*, 2010; Wils *et al.*, 2010; Xu *et al.*, 2010; Swarup *et al.*, 2011), although mutant TDP-43 is more likely to accumulate in the cytoplasm (Swarup *et al.*, 2011). The results of the rodent models suggested that overexpressed nuclear wild-type TDP-43 is toxic, but provide little insight for the significance of mislocalized wild-type TDP-43. Even in mouse models that overexpress wild-type TDP-43 with mutated nuclear localization signals, total human and mouse nuclear TDP-43 was not reduced (Igaz *et al.*, 2011) when compared with that in littermate wild-type controls. Together, these reported mouse models might have a different TDP-43 pathology from that found in patients with ALS. Expecting that a primate model of ALS might more closely reflect the TDP-43 pathology in human patients with ALS, we overexpressed human wild-type TDP-43 in the spinal motoneurons of a non-human primate, the cynomolgus monkey, using an adeno-associated virus (AAV) 1 vector.

Materials and methods

Human subjects

Neurologists clinically diagnosed ALS with the aid of electrophysiological examinations. The clinical diagnosis of definite ALS was based on El Escorial (Brooks *et al.*, 2000) and electrodiagnostic (De Carvalho *et al.*, 2008) criteria and confirmed by neuropathological examination in accordance with published guidelines (Piao *et al.*, 2003).

The patient study protocol was approved by the institutional clinical study committee at Tokyo Medical and Dental University (No. 799). Consent forms for autopsy were obtained from legal representatives of all patients in accordance with the guidelines of the institutional review boards.

Animals

Ten male adult cynomolgus monkeys (*Macaca fascicularis*; 3–7 years old, 3.28–5.10 kg) were bred and treated at Tsukuba Primate Research Centre. The number of monkeys and concentrations of viral stocks were as follows: one monkey was injected with high-dose Flag-TDP-43 AAV1 [1×10^{13} viral genomes (vg)/ml]; six monkeys were injected with low-dose Flag-TDP-43 AAV1 (3×10^{12} vg/ml); three monkeys were injected with low-dose mock AAV1 (3×10^{12} vg/ml) as a negative control. Three monkeys injected with low-dose TDP-43 AAV1 were pathologically examined in the early stage, 3–5 days after the onset of motor symptoms and the other three monkeys were examined in the late stage, 4–7 weeks after injection.

Eleven adult male Fisher rats (10 weeks old, Sankyo-lab) were used. The number of rats and concentrations of viral stocks were as follows: eight rats were injected with low-dose Flag-TDP-43 AAV1 (3×10^{12} vg/ml) and three rats were injected with low-dose control AAV1 (3×10^{12} vg/ml) as a negative control. Three rats injected with TDP-43 AAV1 were pathologically examined in the early stage, 1–2 weeks after injection, and the others were examined in the late stage, 4–9 weeks after injection.

All animal experiments were conducted according to the U.S. National Institutes of Health Guide for the Care and Use of Laboratory Animals, and the Guidelines for the Animal Care and Management of the Tsukuba Primate Research Center and Tokyo Medical and Dental University.

Constructs

Human wild-type TDP-43 was purchased from Invitrogen. The TDP-43 and Flag-TDP-43 fragments were generated by polymerase chain reaction using the following primer pairs: 5′-CCGCTCGAGGCCACCATG GATTAC AAGGATGACGACGATAAGTCTGAATATATTCGGGTAA CCGG-3′ and 5′-CCGCTCGAGCTACATTCCCCAG CCAGAAG ACTTA-3′ for TDP-43, and 5′-CCGCTCGAGGCCACCATGGATTACA AGGATGACGACGAT AAGTCTGAATATATTCGGGTAACCGG-3′ and 5′-CCGCTCGAGCTACATTCCCCAGCCAGAAGACTTA-3′ for Flag-TDP-43, which contained XhoI digestion sites at the 3′- and 5′-ends. The Flag-TDP-43 complementary DNA was subcloned into an expression cassette flanked with AAV2 inverted terminal repeats (Stratagene). The cytomegalovirus (CMV) promoter was used to drive expression.

Adeno-associated virus preparations

Human embryonic kidney (HEK) 293 cells at ~70% confluence were transfected with the AAV1 packaging plasmid pRep2/Cap9 (gift from Dr James M. Wilson, University of Pennsylvania) and adenovirus helper plasmid (Stratagene) at a ratio of 1:1:1. At 6 h after transfection, the culture medium was replaced with fresh medium, and the cells were incubated for 48 h. The cells were then harvested from the culture dishes and pelleted by centrifugation, resuspended in phosphate-buffered saline and subjected to three rounds of freeze–thawing. Cell debris was then pelleted by centrifugation at 1200*g* for 15 min. AAV vectors were purified using ammonium sulphate precipitation and iodixanol (Axis-Shield) continuous gradient centrifugation.

Size-exclusion chromatography was performed using an AKTA Explorer 100 HPLC system (GE Healthcare) equipped with a 2-ml sample loop. A Superdex 200 10/300 GL column (GE Healthcare) was equilibrated with MHA buffer (3.3 mM MES, 3.3 mM HEPES, 3.3 mM NaOAc, 50 mM NaCl, pH 6.5). The vector-containing fractions were loaded onto the column at a flow rate of 0.5 ml/min, and the eluate was collected as 0.5 ml fractions over the duration of one column volume (23 ml). AAV peak fractions were identified by 280/260 nm absorbance and real-time quantitative polymerase chain reaction using vector-specific primers. The purified AAVs were then concentrated further by using Amico Ultra-4 tubes (Ultracel-30k, Millipore) to a final concentration of 1×10^{13} genome copies/ml, as determined by real-time quantitative polymerase chain reaction.

The genome copy number was calculated by TaqMan® PCR (Applied Biosystems). The vectors were treated with Benzonase® and digested with proteinase K (Wako Pure Chemical Industries) for 1 h and purified by phenol–chloroform extraction. The TaqMan® primers and probe were designed as follows: forward primer: 5′-CAGGCTGGT CCAACTCCTA-3′, reverse primer: 5′-GCAGTGGTTCACGCCTGTAA-3′, and probe: 5′-TACCCACCTTGGCCTC-3′. The designed TaqMan® PCR fragment was located in the human growth hormone polyadenylation site in the vector.

Successful viral assembly of control AAV and transgene expression were confirmed by immunoblot analysis using HEK 293 cells infected with AAV (Supplementary Fig. 1), as described below.

HEK-293 cells were cultured in Dulbecco's modified Eagle's medium containing 10% foetal bovine serum with 1% penicillin/streptomycin. The cells in 12-well plates were infected by Flag-TDP-43 AAV1 (5×10^{10} vg/ml). At 48 h after infection, cells were harvested by gentle scraping in lysis buffer [20 mM Tris–HCl, 150 mM NaCl, 1% NP-40, 0.1% deoxicolate, 1% sodium dodecyl sulphate, 1 mM EDTA, 1 mM EGTA, 10 mM β-glycerophosphate, 5 mM NaF and Complete protease inhibitor cocktail (Roche Diagnostics)]. Equal amounts of total cellular protein were mixed with 5× Laemmli sample buffer, denatured at 95°C for 5 min, and separated with 10% sodium dodecyl sulphate polyacrylamide gel electrophoresis. The proteins were transferred to PVDF membranes. After blocking with 3% gelatin (Wako Pure Chemical Industry) in Tris-buffered saline or 5% skimmed milk (Wako Pure Chemical Industry) in Tris-buffered saline-Triton X-100, the membranes were incubated overnight with the following primary antibodies: anti-M2 (1:2000); anti-pan-TDP-43 (1:2000); and anti-VP1, VP2 and VP3 of AAV (1:1000). After incubation with an appropriate horseradish peroxidase-conjugated secondary antibody (Santa Cruz Biotechnology), labelling was detected with the ECL Plus™ Chemiluminescent Detection System (GE Healthcare) or SuperSignal (Thermo Scientific).

Stereotaxic injection of adeno-associated viral vectors

All surgical operations were performed under general anaesthesia. Ketamine hydrochloride (Ketalar, Sankyo) was intramuscularly administered at a dose of 5 mg/kg as a pre-anaesthetic agent, and general anaesthesia was maintained with isoflurane (Forane, Abbott) and oxygen after tracheal intubation. The monkeys were positioned in a stereotaxic frame. After a bilateral laminectomy and opening the dura in the midline at C5–6, AAV vectors were stereotaxically injected into the side ipsilateral to the dominant hand. The injection site was determined and depth of needle insertion was calculated from the preoperatively taken MRI of cervical spinal cord. AAV stock (5 µl) was injected through a 31-gauge needle connected to a 10-µl Hamilton microsyringe in 2 min. The needle remained in place for 10 min and was removed slowly. The dura and skin were sutured and monkeys returned to their individual cages. The monkeys received 0.5 mg/kg butorphanol tartrate (Stadol, Bristol-Myers Squibb) intramuscularly for 3 days to alleviate any postoperative pain.

The rats were anaesthetized with an intraperitoneally administered cocktail of 1.5 ml chloral hydrate (70 mg/ml, Wako Pure Chemical Industry) and 0.1 ml ketamine hydrochloride (70 mg/ml) at a dose of 6 ml/kg. A left side hemi-laminectomy was performed from C4 to C6. On the left side of the C6 segment, 1.5 µl of viral stock was manually injected through sharpened microcapillary glass (PN-30 puller, Narishige) connected via silicone to a 10-µl Hamilton microsyringe at a rate of 0.5 µl/min. The sharpened microcapillary glass remained in place for 3 min and was removed slowly. The skin was sutured, the rats placed on a heating pad until they began to recover from surgery, and then returned to their individual cages.

For detection of the AAV genome in the spinal cord, total DNA was extracted from spinal cord with homogenized buffer containing 0.5% sodium dodecyl sulphate, 10 mM Tris–HCl pH 8.0, and 10 mM EDTA pH 8.0, and polymerase chain reactions were carried out with the following primer pair: 5′-CGCTGTTTTGACCTCCATAGAA-3′ and 5′-AGGCGGTACTTACGTCACTCTTG-3′ for the cytomegalovirus β-globin intron.

Behavioural analysis

For monkeys, to evaluate weakness of the forelimb muscles on the AAV-injected side (the dominant-hand side), we performed the 'apple test'. The front fence of the cage was altered to have two holes and trays on the right and left side. A piece of apple was placed in line from back (monkey side) to front (observer side) on the left or right tray at 3, 6, 9 and 12 cm from the front fence during a session. The monkeys were trained to reach a small piece of apple on the trays through the hole. Four sessions were performed alternately for each side. We analysed how frequently a monkey used his dominant hand to pick up apples before and every week after the operations. We also carefully observed behaviour of the monkeys in daily life every day and recorded video monitoring for 30 min per week.

For rats, to evaluate weakness of the forelimb muscles, we measured grip strength using a special device (Muromachi Kiki) as previously described (Anderson, 2005).

Electrophysiological assessment

The nerve conduction study and needle EMG studies were performed under anaesthesia with a combination of 7 mg/kg ketamine hydrochloride and 1.2 mg/kg xylazine administrated intramuscularly. Nerve conduction studies were performed in the bilateral median nerves using conventional procedures and an EMG Machine (MEB-2300, Nihon-koden). The recording surface electrode was placed over the belly of the thenar eminence with a reference electrode at the metacarpophalangeal joint of the thumb, and compound muscle action potentials were elicited after the stimulation of the median nerve at the wrist. The peak-to-peak amplitudes were measured for all compound muscle action potentials. Nerve conduction studies were examined before AAV injection and every 1 or 2 weeks after. The needle EMG study was performed in the first dorsal interosseous, flexor carpi ulnaris and biceps brachii muscles using a conventional concentric needle electrode used in human studies (TECA Elite, CareFusion), 4–6 weeks after AAV injection.

Neuropathological examinations

Animals were deeply anaesthetized first with intramuscularly administered 7 mg/kg ketamine hydrochloride and then with intravenously administered 25 mg/kg pentobarbital. After confirming the absence of a blink reflex, the spinal cord and skeletal muscles were removed. For neuropathological examination, human and animal spinal cord samples were immersion fixed in 10% neutral buffered formalin, processed conventionally, embedded in paraffin, cut into 4-µm-thick sections and stained with haematoxylin and eosin. For immunostaining, sections were deparaffinized, pretreated in 0.5% periodic acid, autoclaved for 5 min at 121°C and then incubated free-floating overnight at 4°C with the following primary antibodies: M2 (1:500), anti-pan-TDP-43 (1:1000), anti-pS409/410-TDP-43 (1:500), anti-ubiquitin (1:500), anti-p62 (1:500), anti-cystatin-C (1:1000), anti-GFAP (1:500), anti-GLUT-5 (1:500) and SMI31 (1:200). Following brief washes, the sections were sequentially incubated with polymer immunocomplex (Dako)

Immunoreactive elements were visualized by treating sections with 3,3′ diaminobenzidine tetroxide (DAB-4HCl, Dojin Kagaku) with or without nickel ammonium chloride. The sections were then counterstained with haematoxylin. For double-immunostaining, the deparaffinized sections were stained with Sudan Black B to avoid autofluorescence. The free-floating sections were incubated overnight at 4°C in solutions containing the primary antibodies. The sections were then incubated with AlexaFluor 488- or 555-conjugated secondary antibodies (1:500, Invitrogen), and DAPI nuclear stain (1:500, Santa Cruz Biotechnology) for 1 h. All sections were examined using a confocal microscope (NIKON or Carl Zeiss).

Animal anterior root samples were fixed with a mixture of 2.5% glutaraldehyde in 0.1 M phosphate buffer (pH 7.4) at 4°C overnight, and then further fixed in 1% osmium tetroxide in 0.1 M phosphate buffer (pH 7.4) for 1 h. The well-fixed tissues were dehydrated in graded ethanol and embedded in Epon 812 (Poly/Bed® 812, Polyscience). The fixed roots were transversely cut into 1-µm-thick sections and stained with toluidine blue.

For counting of anterior horn neurons in the spinal cord, monkey eighth cervical segments were serially cut at 4-µm thickness, and every fifth section was stained with haematoxylin and eosin. The previous and next serial sections (that is, every fourth and sixth sections) were immunostained with anti-pan-TDP-43 or anti-Flag antibodies. The number and minimum diameters of neurons with nuclei in the lateral or medial nuclear groups in 15 sections were evaluated using the Image J software program from the U.S. National Institutes of Health.

Antibody information

We used the following primary antibodies for immunostaining and immunoblot analyses: mouse monoclonal anti-Flag (M2, Sigma); rabbit polyclonal anti-pan-TDP-43 (10782-1-AP, ProteinTech Group); rabbit polyclonal anti-C-terminal TDP-43 (12892-1-AP, ProteinTech Group); rabbit polyclonal anti-phosphorylated S409/410 TDP-43 (Cosmo Bio); rabbit polyclonal anti-ubiquitin (Dako); rabbit polyclonal anti-cystatin-C (Dako); mouse monoclonal anti-phosphorylated neurofilament (SMI31, Sternberger Monoclonals); rabbit polyclonal anti-glial fibrillary acidic protein (GFAP) (Dako); rabbit polyclonal anti-glucose transporter 5 (GLUT-5, IBL); rabbit polyclonal and mouse monoclonal anti-peripeherin (AB1530 and AB1527, Chemicon); mouse monoclonal anti-neurofilament light (N5139, Sigma) antibody; anti-p62 (GP62-C, Progen); anti-glyceraldehyde-3-phosphate dehydrogenase (GAPDH, Biodesign), and anti-AAV capsid proteins VP1, VP2 and VP3 (Progen Biotechnik).

Sequential biochemical fractionation, dephosphorylation and immunoblot analysis

Frozen frontal cortex or spinal cord (50–250 mg) was homogenized in 10 volumes of buffer A (10 mM Tris–HCl pH 7.5, containing 1 mM

EGTA, 10% sucrose and 0.8 M NaCl). After the addition of Triton X-100 at a final concentration of 1%, the homogenate was incubated for 30 min at 37°C and spun at 100 000*g* for 20 min at 20°C. The pellet was homogenized in 20 volumes of buffer A containing 1% sarkosyl, incubated for 30 min at 37°C and spun at 100 000*g* for 20 min at 20°C. The sarkosyl-insoluble pellet was homogenized in four volumes of buffer A containing 1% CHAPS [3-[(3-cholamidopropyl)dimethylammonio]-1-propanesulphonate] and spun at 100 000*g* for 20 min. The pellet was sonicated in 0.5 volume of 8 mol/l urea buffer, cleared by centrifugation at 100 000*g* for 20 min at 20°C, and used for immunoblotting. The samples before (−) and after (+) treatment with lambda protein phosphatase (1600 U/ml, New England Biolabs) were subjected to 10% sodium dodecyl sulphate polyacrylamide gel electrophoresis. Proteins in the gel were then transferred onto a polyvinylidene difluoride (PVDF) membrane (Millipore). After blocking with 3% gelatin (Wako Pure Chemical Industries) in Tris-buffered saline (50 mM Tris–HCl pH 7.5, 150 mM NaCl), the membranes were incubated overnight with the following primary antibodies: anti-M2 (1:2000); anti-C-TDP-43 (1:1200); anti-phosphorylated S409/410 TDP-43 (1:2000); anti-p62 (1:3000) and anti-GAPDH (1:2000). After incubation with an appropriate horseradish peroxidase-conjugated secondary antibody (Santa Cruz Biotechnology), labelling was detected by a 3,3′diaminobendizene reaction intensified with nickel chloride (Metal-Enhanced DAB Substrate Kit, Thermo Scientific), the ECL Plus™ Chemiluminescent Detection System (GE Healthcare), or SuperSignal (Thermo Scientific).

Quantitative real-time polymerase chain reaction assay

Total RNA was extracted from whole-brain homogenates with Isogen (Nippon Gene). DNase-treated RNA (2.5 μg) was reverse-transcribed with SuperScript® III and random hexamers (Life Technologies). Complementary DNA was amplified by the quantitative TaqMan® system by using the Light Cycler 480 Real-Time PCR Instrument (Roche Diagnostics). The primers and probes specific for Flag-tagged human TDP-43, rat TDP-43 (NM_001011979.2) and monkey TDP-43 (XM_001102660.2) were designed. Relative Flag-human TDP-43 messenger RNA levels were calculated in comparison to endogenous rat or cynomolgus messenger RNA levels. A list of all primers and probes used in this study is provided in Supplementary Table 1.

Statistical analysis

The data obtained from independent experiments are presented as means ± SEM.

Statistical analysis of spinal neuron counts and axonal density among TDP-43-expressed monkey group in early, late stage and control monkey group by one-way ANOVA with Bonferroni's *post hoc* test. $P < 0.05$ was considered significant.

Results

Overexpressing wild-type TDP-43 in the monkey cervical cord leads to progressive motor weakness and muscle atrophy with fasciculation

AAV expressing Flag-tagged TDP-43 (Supplementary Fig. 2) was directly injected into the sixth cervical segment on the dominant-hand side of seven monkeys. All monkeys developed progressive motor weakness and muscle atrophy with marked fasciculation in the forelimb on the injected side (Fig. 1A and B, Supplementary Video 1). Two to 3 weeks after the injection, the TDP-43-expressing monkeys first showed some difficulty in taking time to pick up pieces of apple using the dominant hand on the injected side in the apple test, and changed to use the non-dominant hand (Fig. 1C). On observation by video monitoring, they could reach and grasp the ceiling fence at the onset of clumsiness of picking apples, but 1–3 weeks later could not flex the elbow joint and raise the forelimb, indicating the motor weakness had spread to the proximal muscles (Fig. 1D). In the late stage, 2–5 weeks after the onset, the dominant hand muscles became completely paralysed (Fig. 1A), and muscle weakness and atrophy had spread to the contralateral, un-injected side limb muscles (Fig. 1B and E). One of TDP-43-expressing monkeys showed respiratory failure at the end stage. The control monkeys did not show obvious motor symptoms, indicating surgical procedure or virus toxicity was minimal (Fig. 1C–E and Supplementary Video 2).

Electrophysiological findings

Electrophysiologically, in all TDP-43-expressing monkeys, the compound muscle action potential of the thenar muscle evoked by stimulation of the median nerve at the wrist progressively decreased in size with preservation of conduction velocity, and the muscle became unexcitable in the late stage (Fig. 2A). In contrast, three monkeys injected with control AAV did not show a marked change compound muscle action potential size (Fig. 2A). In TDP-43-expressing monkeys, the compound muscle action potential size on the contralateral side was not changed in the early stage (3–5 days after the onset of motor symptoms), but showed milder reduction of compound muscle action potential size in the late stage (Fig. 2B). Needle EMG revealed robust fasciculation potentials, and denervating potentials of positive sharp waves and fibrillation potentials in the late stage (Fig. 2C).

Cytoplasmic mislocalization with loss of endogenous monkey TDP-43, dystrophic neurites and cystatin C-positive granules in the cytoplasm

Neuropathologically, an anti-Flag antibody widely detected exogenous TDP-43 in neurons from the second cervical to the second thoracic segments on both sides, and was observed in almost all neurons on the injected side from the fourth to eighth cervical segments. Generally, Flag immunoreactivity was not detected in the glial cells. There was no inflammatory reaction except for in the area around the injection site. In the late stage, exogenous TDP-43 was observed in either the nucleus or cytoplasm (Fig. 3A). Pan-TDP-43 staining revealed that most motoneurons with cytoplasmic TDP-43 lost endogenous monkey TDP-43 staining (Fig. 3B), which normally localized in the nucleus (Fig. 3C). Mislocalized TDP-43 was diffusely distributed in the cytoplasm

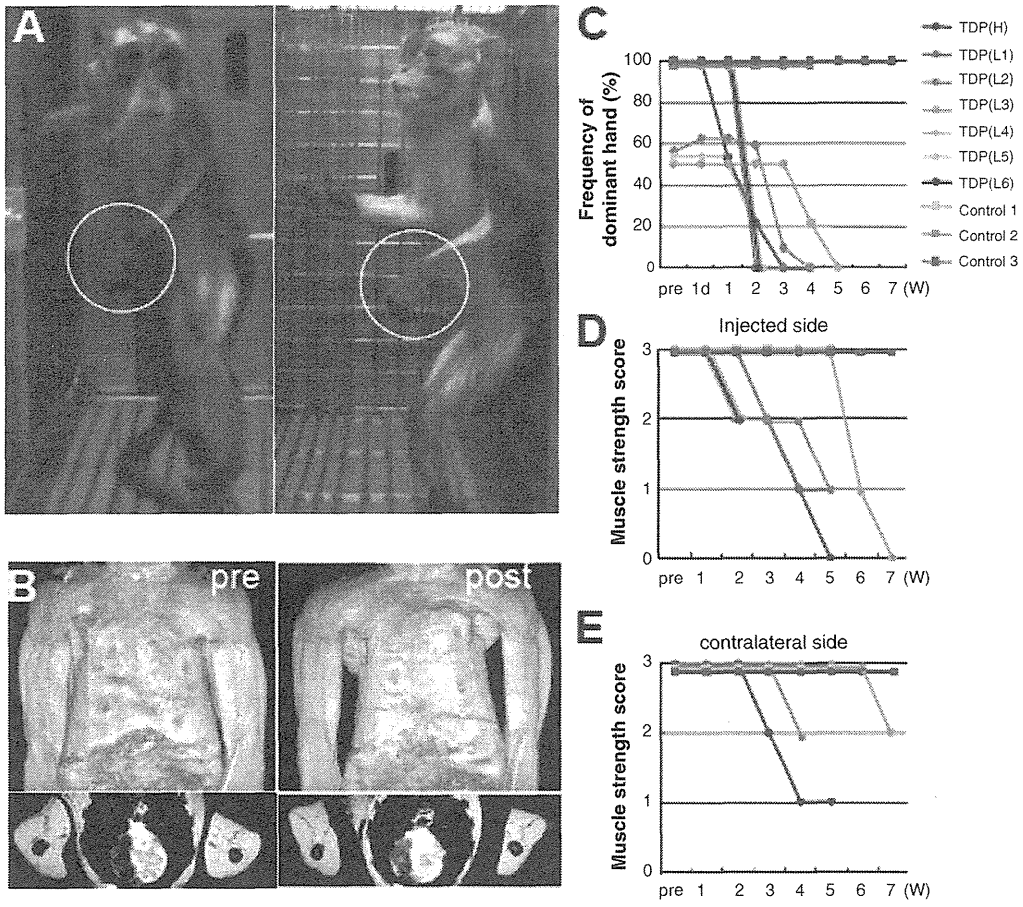

Figure 1 Overexpressing wild-type TDP-43 in the monkey cervical cord leads to progressive motor weakness and muscle atrophy. (**A**) Motor paresis of the forelimb on the injected side (encircled) in TDP-43 AAV-injected monkeys. (**B**) Constructed (*top*) and axial (*bottom*) MRI images of upper arm muscles before (pre) and 4 weeks after (post) injection, indicating a marked muscle atrophy of upper and forearms as well as hand muscles, predominantly on the injected side (left side). (**C**) Apple test. Frequency with which the dominant hand was used to pick up apples. (**D** and **E**) Behavioural analysis assessing muscle strength of forearms on the injected side (**D**) and contralateral side (**E**). A score of 3 indicates that the monkeys can hang on the ceiling fence; score of 2, they can grasp but not hang on the ceiling fence; score of 1, they can raise the forelimb but not reach ceiling fence; score of 0, they cannot raise the forelimb. Measurements that appear to end before the end of the experiment are from the three monkeys that were pathologically examined in the early stage.

and, in some neurons, granularly aggregated (Fig. 3B). Proximal and distal dystrophic neurites were occasionally observed (Fig. 3A and B). Phosphorylation of TDP-43 in the nucleus or cytoplasm was not clear in the early stage, but became obvious in the late stage (Fig. 3D). Anti-ubiquitin and anti-p62 antibodies did not show a clear abnormal signal. Astrogliosis and microgliosis were observed (Supplementary Fig. 3). A small fraction of the motoneurons expressing TDP-43 in the nucleus characteristically displayed coarse cystatin C-positive granules in the cytoplasm (Fig. 3E) in the neurons with exogenously expressed TDP-43 in the nucleus. There were no neurons with co-localized cystatin C-positive granules and TDP-43 aggregates in the cytoplasm. We also observed aberrant accumulation of phosphorylated neurofilaments (Fig. 3F) and peripherin (Supplementary Fig. 4) in the cytoplasm of spinal motoneurons, a common pathological feature in patients with ALS (Munoz *et al.*, 1988; Corbo and Hays, 1992). Immunostaining with an anti-Flag antibody identified its nuclear or cytoplasmic immunoreactivity in some Betz cells in the precentral gyrus restricted to the forelimb area contralateral to the injection. This Flag immunoreactivity was not observed in other cortical areas (including hippocampus and frontal lobe, which are preferentially affected in patients with FTLD), thalamus, basal ganglia and white matter, or in glial cells (Supplementary Fig. 5).

Characteristic regional mislocalization of TDP-43 in motoneurons of the anterior horn similar to amyotrophic lateral sclerosis spinal cords

In the early stage, 3–5 days after the onset of hand clumsiness, TDP-43 mislocalization of diffuse staining pattern was observed in

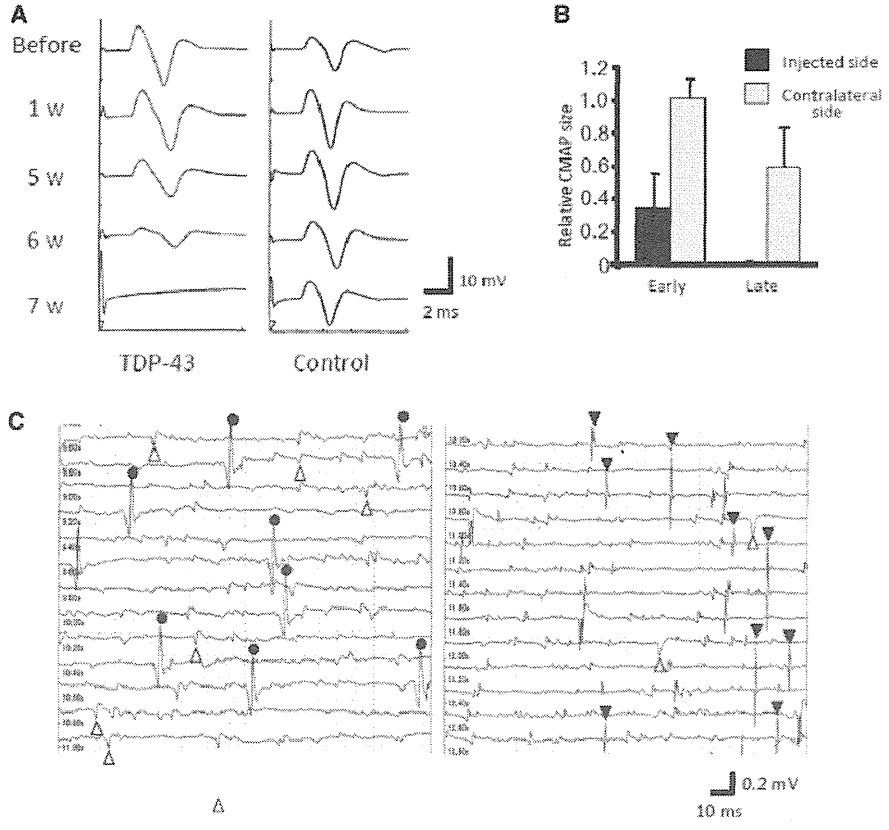

Figure 2 Electrophysiological findings for motor symptoms of the monkeys. (**A**) Compound muscle action potentials (CMAPs) in the thenar muscle after stimulation of the median nerve at the wrist. They gradually decreased in size, and became inexcitable in the late stage. There was no change of compound muscle action potential size in the control monkey. (**B**) Ratio of the compound muscle action potential size 3–5 days after the onset (early stage) or 2–5 weeks after the onset (late stage) to the size before injection. In the early stage, there was no reduction in compound muscle action potential size on the contralateral side, but moderately attenuated in the late stage. (**C**) Needle EMG findings of the forearm muscle. Circles indicate fasciculation potentials; open triangles, positive sharp waves; filled triangles, fibrillation potentials.

most motoneurons in the lateral nuclear group of the anterior horn. In contrast, almost all neurons in other areas of the spinal cord including the posterior horn showed flag signal of exogenously expressed TDP-43 only in the nucleus (Fig. 4A and D). Importantly, the contralateral lateral nuclear group also exhibited TDP-43 mislocalization on the side of forelimb that did not yet show obvious motor symptoms (Supplementary Fig. 6). Signals of exogenous Flag-TDP-43 were detected by real-time polymerase chain reaction on the contralateral half of the spinal cord (Supplementary Fig. 7). However, this distribution indicates that this regional selectivity is not due to differences in the concentration of the injected AAV, but rather is due to properties of the affected neurons. In the late stage, 2–5 weeks after onset, the percentage of motoneurons with TDP-43 mislocalization decreased ~47% in the lateral nuclear group, and was <2% in the ventromedial nuclear group (Figs 3B and 4D). The number of large motoneurons (⩾20 μm) in the early stage in this lateral nuclear group did not change, but in the late stage, was reduced by ~42% (Fig. 4B, C and E). In contrast, the reduction in the number of large neurons in the ventromedial nuclear group was not significant (control, 1.78 ± 0.20 versus TDP-43, 1.68 ± 0.18/section, $P = 0.80$). Astrogliosis was also more prominent in the lateral area than in the ventromedial area of the anterior horn (data not shown). Motoneuronal degeneration of the lateral nuclear group was also confirmed by studying the anterior roots of the eighth cervical segment, which showed frequent myelin ovoids and loss of large myelinated axons (⩾8 μm) in the late stage, although they were almost normal in the early stage (Fig. 5A–C). This axonal loss in the anterior roots is consistent with pathological change of the thenar muscle, showing numerous small angulated atrophic fibres (Fig. 5D).

We furthermore examined whether such a regional change of TDP-43 mislocalization occurs in spinal cord of nine patients with ALS with upper limb weakness and hand muscle atrophy. TDP-43 mislocalization was observed much more in the lateral nuclear group than in the ventromedial nuclear group of the cord at the eighth cervical segment (Fig. 6A–C).

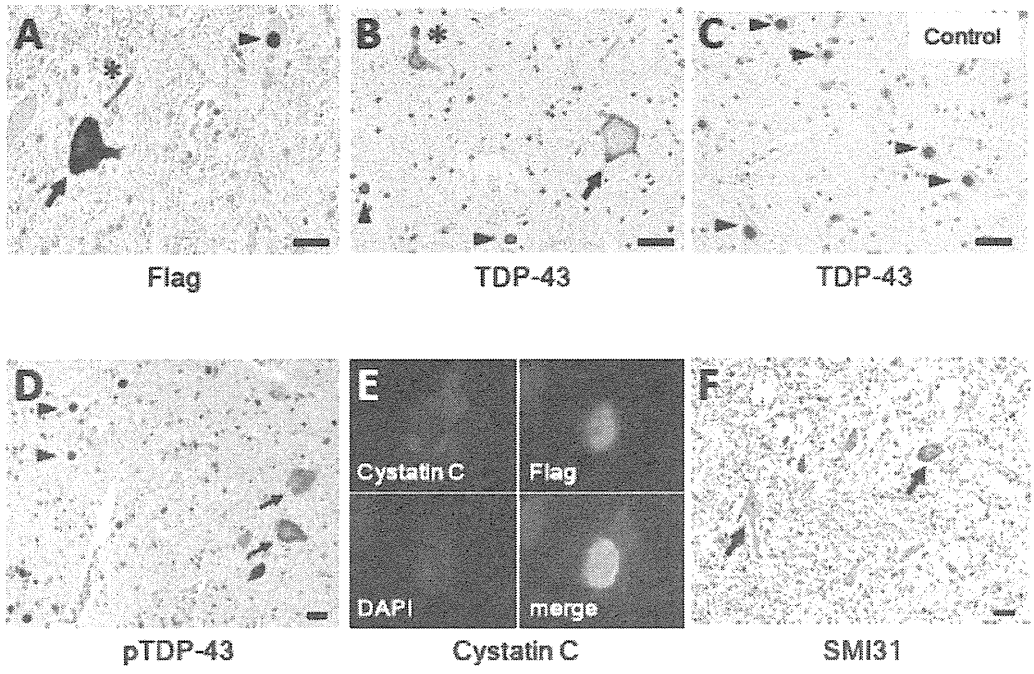

Figure 3 Neuropathological findings of monkey spinal cords of TDP-43–overexpressed monkeys at the late stage (**A**, **D–F**), and control with mock AAV (**C**). (**A–D**) TDP-43-overexpressed spinal cord immunostaining using antibodies to Flag (**A**), pan-TDP-43 (**B**) and pS409/410 TDP-43 (**D**) demonstrated mislocalization in cytoplasm (arrows), and dystrophic neurites (asterisks) as well as normal localization in nuclei (arrowheads), whereas normal spinal cord showed only nuclear localization of TDP-43. (**E**) Co-labelling of a motoneuron expressing TDP-43 in the nucleus with antibodies to cystatin C (red) and Flag (green). The nucleus is labelled with DAPI. (**F**) Immunostaining using SMI31 revealed the aberrant presence of phosphorylated neurofilament in the neuronal cytoplasm (arrows). Scale bars: 20 μm. Immunostainings of spinal cord with control mock AAV using the antibodies to Flag, pS409/410 TDP-43, cystatin C and SMI31 are shown in Supplementary Fig. 7.

Interspecies differences in TDP-43 pathology in rodents and primates

To investigate interspecies differences in TDP-43 pathology, we injected the identical TDP-43-expressing AAV at the same concentration into rat cervical cords. Expression level of Flag-TDP-43 messenger RNA around the injection site in rat spinal cord was >20-fold higher than that of endogenous TDP-43 level, and this fold change was similar to that in monkey spinal cord (Fig. 7A). Rats injected with TDP-43 AAV showed progressive motor weakness (Fig. 7B), measured by grip strength. Importantly, exogenous TDP-43 was observed only in the nuclei of motoneurons in both early (14 days after injection of AAV) and late (4 weeks after injection of AAV) stages (Fig. 7C). Since mislocalization of TDP-43 in the monkey spinal cords was more prominent in the early stage (14 days), we also examined the pathology of rat spinal cords at a very early stage (7 days); however, the weak Flag immunoreactivity was still limited to the nucleus of motoneurons (data not shown). Furthermore, this rat model failed to exhibit cystatin C-positive aggregates, dystrophic neurites, or aberrant accumulation of phosphorylated neurofilaments in the cytoplasm of spinal motoneurons (Fig. 7D). These neuropathological findings indicate that this rat model was less similar to human ALS than our monkey model in TDP-43 localization and other characteristic features of ALS.

Detection of the 25-kDa C-terminal fragment and phosphorylated TDP-43 in the early stage

Biochemically, immunoblot analysis of monkey spinal cord demonstrated that the exogenous Flag-tagged TDP-43 became much more insoluble than endogenous TDP-43 (Fig. 8A). The phosphorylation of TDP-43 was unclear in the early stage (Fig. 8B) but clearly detected later (Fig. 8C). Neither a C-terminal nor a phosphospecific TDP-43 antibody detected the 25-kDa C-terminal fragment (Fig. 8A–C). These suggest that neither phosphorylation of TDP-43 or its 25-kDa C-terminal fragment in spinal cord is necessary to initiate motoneuronal dysfunction and degeneration in our monkeys.

Discussion

Frequent mislocalization of TDP-43 in the cytoplasm and loss of its nuclear staining are major pathological hallmarks in the histological

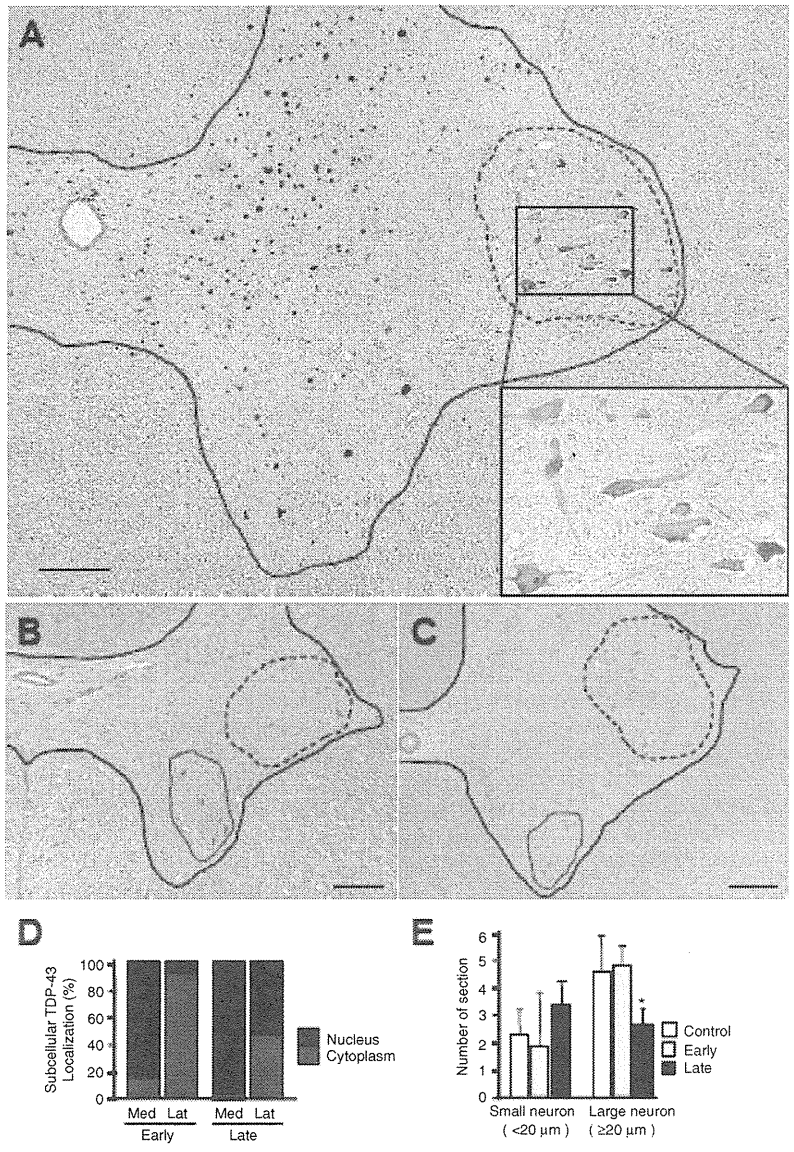

Figure 4 Regional mislocalization of TDP-43 and cell death in monkey spinal cords. (**A**) Sections from the injected side of the eighth cervical segment of the cord taken at the early stage and immunostained with an anti-Flag antibody. Most neurons in the lateral nuclear group (area encircled by broken line) showed cytoplasmic mislocalization of TDP-43 (inset), but almost all neurons in other areas expressed exogenous TDP-43 in the nucleus. Scale bars: 200 μm. (**B** and **C**) The eighth cervical level of cord from monkeys injected with TDP-43–expressing (**B**) and control (**C**) AAV, taken at the late stage and stained with haematoxylin and eosin. The number of large motoneurons decreased in the lateral nuclear group (areas encircled by broken line), but not in ventromedial nuclear group (areas encircled by red solid line). Scale bars: 200 μm. (**D**) Percentage of neurons with nuclear (black) or cytoplasmic (red) localization of exogenous TDP-43 in the lateral nuclear groups on the injected side. Neurodegeneration affects the lateral nuclear group more than the ventromedial nuclear group. (**E**) Cell count of neurons in the lateral nuclear group on haematoxylin and eosin staining. Mean ± SEM. $n = 3$, $^*P < 0.05$. Lat = lateral nuclear group; Med = ventromedial nuclear group.

diagnosis of ALS and FTLD (Geser *et al.*, 2010). The classification of TDP-43 proteinopathy is based on a combination of neuronal cytoplasmic inclusions and dystrophic neurites (Mackenzie *et al.*, 2011). The morphological features in our monkeys are close to type B TDP-43 proteinopathy, which is usually observed in the brains of patients with ALS. The only difference between the pathology of our monkeys and type B TDP-43 proteinopathy is that mislocalized cytoplasmic TDP-43 was usually diffuse and neuronal cytoplasmic inclusions were less frequent in our monkeys. Since this monkey is an acute model for TDP-43 pathology, it possibly

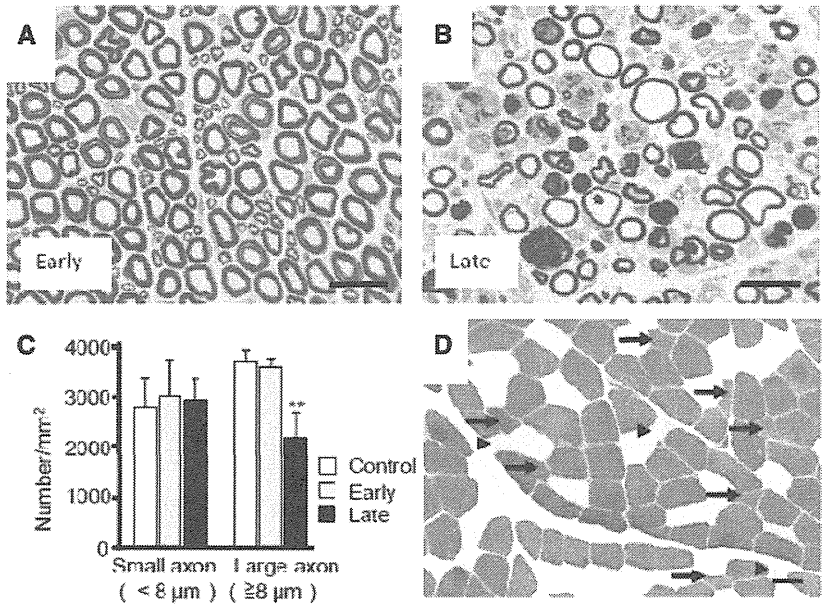

Figure 5 Pathological finding of monkey anterior root and skeletal muscle. Toluidine blue staining of the eighth cervical anterior roots on the injected side in the early (**A**) and late (**B**) stages, and their myelinated axon densities (**C**). Mean ± SEM, $n = 3$, $^{**}P < 0.01$. (**D**) Transverse section of the biceps brachii muscle from a TDP-43–expressing monkey 4 weeks after injection, stained with ATPase (pH 10.6). Small angulated atrophic changes of type I (arrowheads) and type II (arrows) fibres, with predominant involvement of type II fibres, can be seen. Scale bar: 50 μm.

takes more time for diffusely mislocalized TDP-43 to be aggregated. Moreover, in the spinal cords of patients with ALS, diffuse cytoplasmic TDP-43 staining is more common, and neuronal cytoplasmic inclusions are less frequent than in the brain and may even be absent (Giordana *et al.*, 2010). Thus, our monkey model shows the key features of TDP-43 proteinopathy as seen in the ALS spinal cord.

Interestingly, despite the diffuse expression of exogenous TDP-43 in the spinal cord, TDP-43 mislocalization and neuron loss predominantly occurred in the lateral nuclear group in Rexed lamina IX, in which large neurons are mostly α-motoneurons (Carpenter *et al.*, 1983). The sensory neurons and interneurons in laminae III–VIII rarely showed TDP-43 mislocalization, and large motoneurons in the ventromedial nuclear group, most of which are also α-motoneurons, showed much less TDP-43 mislocalization and neuron loss. Within lamina IX, the lateral nuclear group innervates the distal, fast-contracting muscles of the extremities, and the ventromedial nuclear group innervates the posture-related, continuously contracting muscles attached to the axial skeleton (Carpenter *et al.*, 1983). This regional vulnerability among α-motoneurons is consistent with the distal hand or foot muscles being the first involved in 73% of patients with non-bulbar ALS (Harverkamp *et al.*, 1995; Körner *et al.*, 2011) and might be related to axon length, which affects axonal transport (Bilsland *et al.*, 2010), or to the preferential susceptibility of fast-fatigue rather than slow motoneurons (Dengler *et al.*, 1990; Pun *et al.*, 2006). Furthermore, in nine patients with ALS, more TDP-43 mislocalization was observed in the lateral nuclear group than in the ventromedial nuclear group of the eighth cervical cord segments. Taking these results together, we think that the tropism of TDP-43 mislocalization was similar to that of ALS pathology. However, expression levels of exogenous wild-type TDP-43 in our monkey and rat models were very high (~20-fold higher than that of endogenous TDP-43), which was partly due to lack of 3′-untranslated region in our TDP-43 expression construct. This is probably because TDP-43 controls its own expression through a negative feedback loop by binding to 3′-untranslated region sequences in its own messenger RNA (Ayala *et al.*, 2010; Polymenidou *et al.*, 2010). The unphysiologically high level of TDP-43 expression in our animal models should be taken into consideration when interpreting our findings.

Since Flag TDP-43 messenger RNA was detected in the spinal cord contralateral to the injected side by real-time polymerase chain reaction analysis, the AAV virus was shown to spread contralaterally through the spinal cord causing motor paresis and reduction of compound muscle action potential size in the opposite forelimb. However, it is still possible that there was concomitant cell-to-cell or trans-synaptic propagation of Flag TDP-43 protein in the spinal cord. Moreover, it is interesting that the Flag-TDP-43 signal was selectively extended into Betz cells in the forelimb area of precentral gyrus contralateral to the injection side, which can be explained by a retrograde progression from α-motoneuron in the cervical cord. More sophisticated experimental paradigms are necessary to distinguish whether it is the AAV vector itself,

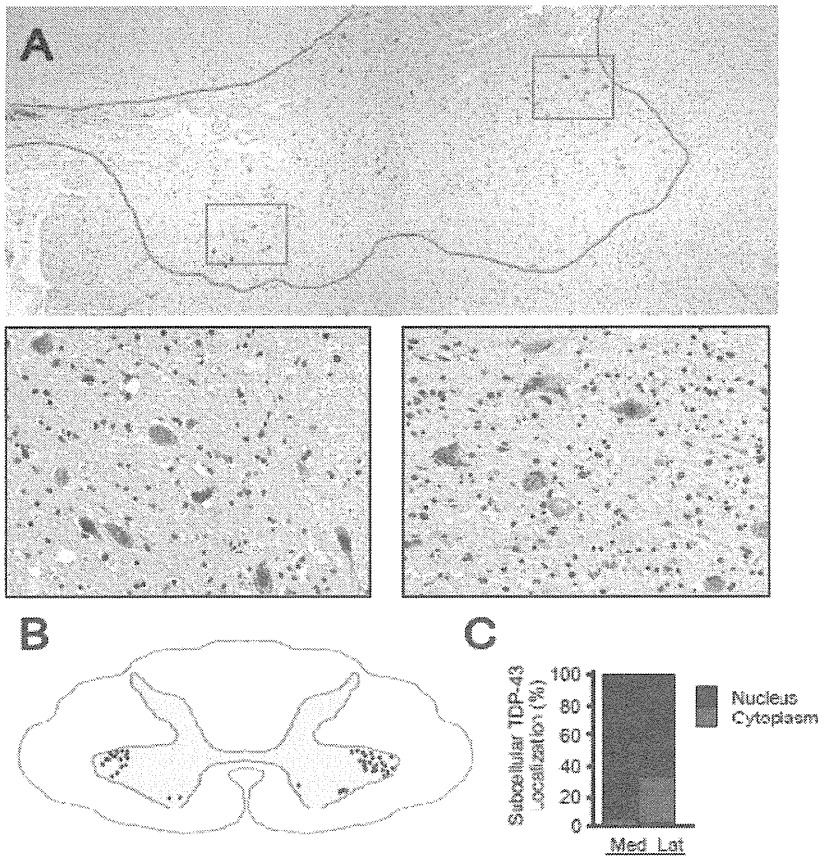

Figure 6 Pan-TDP-43 staining of spinal cords of patients with ALS. (**A**) Autopsied eighth cervical segment of spinal cord immunostained with pan-TDP-43 antibody. Scale bars: 200 μm in **A** and 50 μm in window insets. (**B**) Schematic illustration of the distribution of neurons with TDP-43 mislocalization, made by summing data from five sections (at 20-μm intervals). (**C**) Percentage of neurons with nuclear or cytoplasmic localization of exogenous TDP-43 in the lateral and medial nuclear groups. More frequent TDP-43 mislocalization in the lateral nuclear group in spinal cords of patients with ALS than in the medial nuclear group. Mean ± SEM, $n = 10$, $P < 0.01$. Scale bars: 50 μm. Lat = lateral nuclear group; Med = ventromedial nuclear group.

transcribed messenger RNA or Flag-TDP protein that is the molecule responsible for this progression, which is a prime objective for our future study.

Bunina bodies are small, cystatin C-positive, eosinophilic cytoplasmic inclusions and are generally considered a specific hallmark of sporadic ALS (Okamoto *et al.*, 1993; Mitsumoto *et al.*, 1998). Importantly, Bunina bodies are absent in familial ALS that is due to the SOD1 mutation (Tan *et al.*, 2007) or FUS/TLS mutation (Tateishi *et al.*, 2010), but they have been detected in familial ALS with the TDP-43 mutation (Yokoseki *et al.*, 2008) as well as in sporadic ALS. These imply an association between Bunina bodies and TDP-43 pathology in sporadic ALS. From this point of view, the generation of cystatin C-positive cytoplasmic aggregates in our monkeys might strengthen their pathological value as a model of sporadic ALS.

Biochemically, TDP-43 proteinopathy is characterized by decreased solubility, phosphorylation and the generation of 25-kDa C-terminal fragment (Arai *et al.*, 2006; Neumann *et al.*, 2006; Hasegawa *et al.*, 2008). In TDP-43-overexpressing monkeys, the exogenous TDP-43 became much more insoluble than endogenous TDP-43 of control monkeys, indicating that expression of large amounts of exogenous wild-type TDP-43 can render it insoluble. Unexpectedly, the solubility of endogenous monkey TDP-43 did not become insoluble in TDP-43-overexpressing monkeys. The expectation would be that exogenous insoluble TDP-43 would recruit endogenous monkey TDP-43 and alter its solubility. In this biochemical aspect of TDP-43 solubility, our monkey model differs from patients with ALS.

The pathological role of phosphorylated TDP-43 is still unclear; TDP-43 phosphorylation in culture cells enhances its oligomerization (Hasegawa *et al.*, 2008), but experiments with a phosphorylation-resistant mutant TDP-43 indicated that phosphorylation is not required for inclusion formation or cellular toxicity (Zhang *et al.*, 2009). In our monkeys, phosphorylation of TDP-43 was a late event but not observed at 4 days after symptom onset. This finding suggests that TDP-43 phosphorylation is not

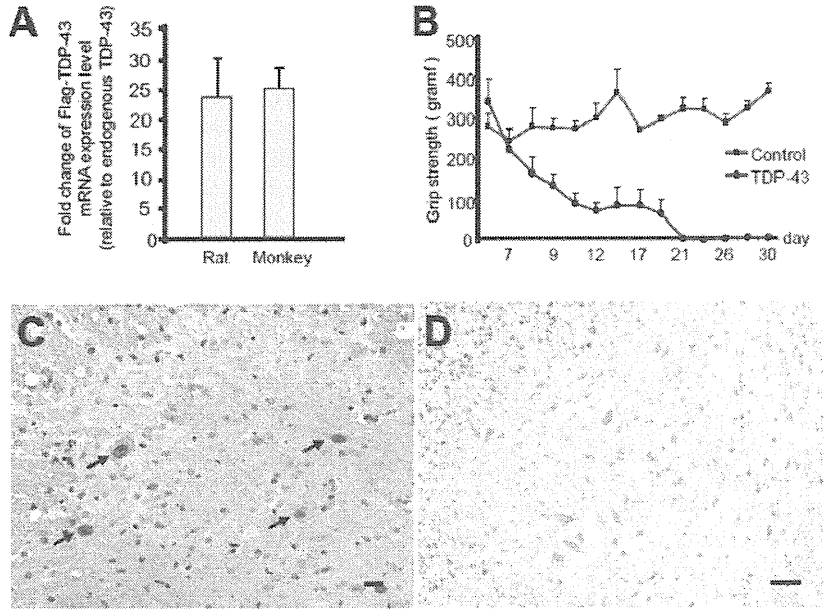

Figure 7 Effect of TDP-43-expressing AAV in rat spinal cords. (**A**) Ratio of exogenously expressed Flag-TDP-43 messenger RNA level to endogenous rat or cynomolgus TDP-43 messenger RNA level evaluated by quantitative real-time polymerase chain reaction. Mean ± SEM, rat, $n = 4$; cynomolgus, $n = 3$, $P = 0.74$. (**B**) Time course of grip strength. Mean ± SEM. (**C**) Nuclear staining of exogenous TDP-43 in cervical cord sections of AAV-injected rats by immunostaining with an anti-Flag antibody (arrows). (**D**) Immunostaining of cervical cord sections of TDP-43–expressing rat, 4 weeks after injection, with SMI31 did not show aberrant phosphorylated neurofilament in the neuronal cytoplasm. Scale bars: 20 μm.

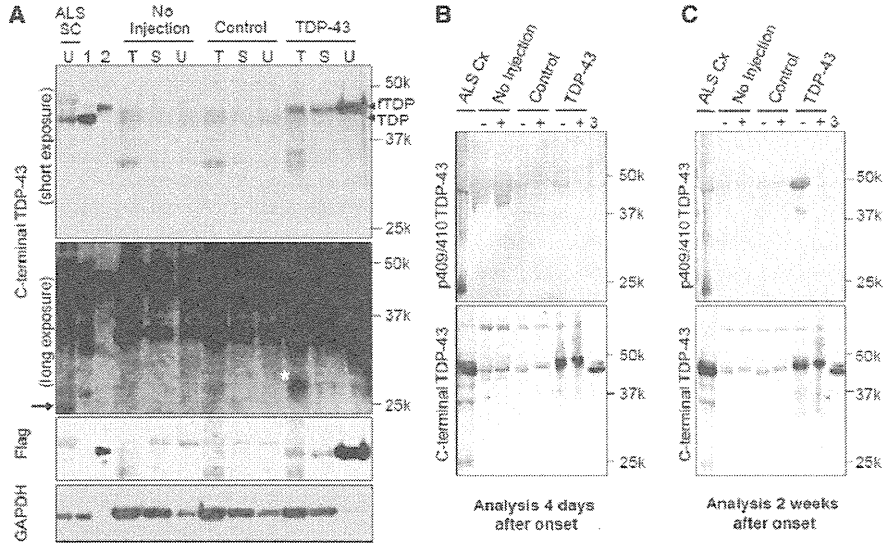

Figure 8 Biochemical analysis of monkey spinal cords. (**A**) Immunoblot of cervical spinal cord lysates from TDP-43–expressing monkeys (4 weeks after injection) and patients with ALS using antibodies recognizing the C-terminus of TDP-43 and Flag. SC = spinal cord of patient with ALS; 1 = TDP-43–expressing HEK 293 T cell lysate; 2 = Flag-TDP-43–expressing HEK 293T cell lysate; T = 1% Triton X-100-soluble; S = 1% sarkosyl-soluble; U = 8 mol/l urea-soluble fraction; fTDP = Flag-TDP-43. A longer exposure (second panel from *top*) revealed the 25-kDa C-terminal fragment in the spinal cord of a patient with ALS (arrow). The ~30-kDa band noted in the Triton-soluble fraction from the spinal cord of a TDP-43–expressing monkey (asterisk) was different from the 25-kDa C-terminal fragment (arrow). (**B** and **C**) Immunoblot of 8 mol/l urea-soluble fraction from the monkey spinal cord harvested 4 days (**B**) and 2 weeks (**C**) after onset of symptoms, using antibodies to pS409/410 TDP-43 (*top*) and C-TDP-43 (*bottom*) before (−) and after (+) treatment with lambda protein phosphatase (λPPase). 3 = Mixture of Flag-TDP-43- and TDP-43-expressing HEK 293T cell lysates. The phosphorylated TDP-43 was detected only in the late stage (asterisk).

necessary to initiate motor symptoms and is a late event in motoneuron degeneration.

In the spinal cords of our monkeys, neither a C-terminal nor a phosphospecific TDP-43 antibody detected the 25-kDa C-terminal fragment that is found in patients with ALS. Overexpressed 25-kDa C-terminal fragment in cultured cells is reported to be toxic (Igaz *et al.*, 2009; Zhang *et al.*, 2009), and the accumulation of 25-kDa C-terminal fragment in transgenic mouse brain correlates with disease progression (Xu *et al.*, 2010). Interestingly, unlike the FTLD/ALS brain, the 25-kDa C-terminal fragment is often absent in the ALS spinal cord (Neumann *et al.*, 2009). The absence of 25-kDa C-terminal fragment in ALS spinal cord does not necessarily preclude a primary role for this form; rather it can be pathologically crucial if its absence is due to the accelerated degeneration of motoneurons with 25-kDa C-terminal fragment. It is difficult to deny that small amounts of C-terminal truncated species are actually present, because mislocalization of TDP-43 was focal in the spinal cord of our monkeys. However, the failure to detect 25-kDa C-terminal fragment in our monkey spinal cord at the early stage may have an implication that full-length TDP-43 is sufficient to be toxic, because α-motor axonal excitability was impaired but their cell bodies were preserved at autopsy.

The results of studies on the relationship between TDP-43 mislocalization and neuron loss remain controversial. The overexpression of wild-type TDP-43 in the nuclei in a transgenic rodent model was sufficient to be toxic to spinal motoneurons (Li *et al.*, 2010; Shan *et al.*, 2010; Wils *et al.*, 2010; Xu *et al.*, 2010), which is consistent with our observations in the rat model. In this context, it can be interpreted that the cytoplasmic mislocalization of wild-type TDP-43 is an epiphenomenon and not a necessary condition for the disease. However, in our monkey model, TDP-43 mislocalization was detected in almost all of the large motoneurons of the lateral nuclear group at the early or even the presymptomatic stage, and these motoneurons later showed neuron loss. In contrast, overexpressed exogenous TDP-43 in the large motoneurons of the ventromedial nuclear group was restricted to the nucleus, but did not produce neuron loss. Mice with over-expression of human TDP-43 engineered to localize in the cytoplasm showed progressive neuronal loss and downregulation of endogenous nuclear mouse TDP-43 expression (Igaz *et al.*, 2011). These suggest that TDP-43 mislocalization is an upstream event in the cascade of motoneuronal degeneration. This finding is consistent with the observation that the highest percentage of neurons with TDP-43 mislocalization was found in the early stage of ALS in patients (Giordana *et al.*, 2010).

In conclusion, our monkey model is superior to rodent models in recapitulating the TDP-43 pathology and in the presence of Bunina body-like inclusion and is expected to be a powerful tool for investigating developing effective therapies as well as the disease pathogenesis of sporadic ALS.

Acknowledgements

The authors are grateful to Drs Masato Hasegawa, Makoto Urushitani and Hiroshi Tsukagoshi for discussion and technical advices on Western blotting and pathological analysis; Dr Takashi Shimada, and Ms Fumiko Sunaga for AAV preparation; Dr Satoshi Ikeda, Dr Masumi Ichikawa, Dr Kinya Ishikawa, Miss Tomoko Ueno, Miss Minako Suzuki, Ms Michiko Imanishi, and Ms Hiromi Kondo for technical support on pathological analysis; Dr Kazuo Kusano for surgical support; Ms Yuki Yamamoto, Dr Miho Akaza for their help.

Funding

Comprehensive Research on Disability Health and Welfare (Grant Nos 20301501 and 23161501 to T.Y. and H.M.); Research on Neurodegenerative Diseases/ALS from Ministry of Health, Labor and Welfare, Japan; Grant-in-Aid for Scientific Research (A) (Grant No. 22240039 to T.Y.) and Grant-in-Aid for Research Activity Start-up (Grant No. 22890051 to T.T.) and Strategic Research Program for Brain Science, Field E from Ministry of Education, Culture, Sports and Technology, Japan.

Supplementary material

Supplementary material is available at *Brain* online.

References

Anderson KD, Gunawan A, Steward O. Spinal pathways involved in the control of forelimb motor function in rats. Exp Neurol 2005; 194: 161–74.

Arai T, Hasegawa M, Akiyama H, Ikeda K, Nonaka T, Mori H, et al. TDP-43 is a component of ubiquitin-positive tau-negative inclusions in frontotemporal lobar degeneration and amyotrophic lateral sclerosis. Biochem Biophys Res Commun 2006; 351: 602–11.

Ash PE, Zhang YJ, Roberts CM, Saldi T, Hutter H, Buratti E, et al. Neurotoxic effects of TDP-43 overexpression in *C. elegans*. Hum Mol Genet 2010; 19: 3206–18.

Ayala YM, De Conti L, Avendaño-Vázquez SE, Dhir A, Romano M, D'Ambrogio A, et al. TDP-43 regulates its mRNA levels through a negative feedback loop. EMBO J 2011; 30: 277–88.

Bilsland LG, Sahai E, Kelly G, Golding M, Greensmith L, Schiavo G. Deficits in axonal transport precede ALS symptoms in vivo. Proc Natl Acad Sci USA 2010; 107: 20523–8.

Brooks BR, Miller RG, Swash M, Munsat TL. El Escorial revisited: revised criteria for the diagnosis of amyotrophic lateral sclerosis. Amyotroph Lateral Scler Other Motor Neuron Disord 2000; 1: 293–9.

Buratti E, Baralle FE. Characterization and functional implications of the RNA binding properties of nuclear factor TDP-43, a novel splicing regulator of CFTR exon 9. J Biol Chem 2001; 276: 36337–43.

Buratti E, Baralle FE. Multiple roles of TDP-43 in gene expression, splicing regulation, and human disease. Front Biosci 2008; 13: 867–8.

Buratti E, De Conti L, Stuani C, Romano M, Baralle M, Baralle F. Nuclear factor TDP-43 can affect selected microRNA levels. FEBS J 2010; 277: 2268–81.

Cairns NJ, Neumann M, Bigio EH, Holm IE, Troost D, Hatanpaa KJ, et al. TDP-43 in familial and sporadic frontotemporal lobar degeneration with ubiquitin inclusions. Am J Pathol 2007; 171: 227–40.

Carpenter MB, Sutin J. Human neuroanatomy. 8th edn. Baltimore: Williams & Wilkins; 1983.

Corbo M, Hays AP. Peripherin and neurofilament protein coexist in spinal spheroids of motor neuron disease. J Neuropathol Exp Neurol 1992; 51: 531–7.

De Carvalho M, Dengler R, Eisen A, England JD, Kaji R, Kimura J, et al. Electrodiagnostic criteria for diagnosis of ALS. Clin Neurophysiol 2008; 119: 497–503.

Dengler R, Konstanzer A, Küther G, Hesse S. Amyotrophic lateral sclerosis: Macro–EMG and twitch forces of single motor units. Muscle Nerve 1990; 13: 545–50.

Geser F, Lee VM, Trojanowski JQ. Amyotrophic lateral sclerosis and frontotemporal lobar degeneration: A spectrum of TDP-43 proteinopathies. Neuropathology 2010; 30: 103–12.

Giordana MT, Piccinini M, Grifoni S, De Marco G, Vercellino M, Magistrello M, et al. TDP-43 redistribution is an early event in sporadic amyotrophic lateral sclerosis. Brain Pathol 2010; 20: 351–60.

Gitcho MA, Bigio EH, Mishra M, Johnson N, Weintraub S, Mesulam M, et al. TARDBP 3'-UTR variant in autopsy-confirmed frontotemporal lobar degeneration with TDP-43 proteinopathy. Acta Neuropathol 2009; 11: 633–45.

Hanson KA, Kim SH, Wassarman DA, Tibbetts RS. Ubiquilin modifies TDP-43 toxicity in a Drosophila model of amyotrophic lateral sclerosis (ALS). J Biol Chem 2010; 285: 11068–72.

Harverkamp LJ, Appel V, Appel SH. Natural history of amyotrophic lateral sclerosis in a data base population. Validation of a scoring system and a model for survival prediction. Brain 1995; 118: 707–19.

Hasegawa M, Arai T, Nonaka T, Kametani F, Yoshida M, Hashizume Y, et al. Phosphorylated TDP-43 in frontotemporal lobar degeneration and amyotrophic lateral sclerosis. Ann Neurol 2008; 64: 60–70.

Igaz LM, Kwong LK, Chen-Plotkin A, Winton MJ, Unger TL, Xu Y, et al. Expression of TDP-43 C-terminal fragments in vitro recapitulates pathological features of TDP-43 proteinopathies. J Biol Chem 2009; 284: 8516–24.

Igaz LM, Kwong LK, Lee EB, Chen-Plotkin A, Swanson E, Unger T, et al. Dysregulation of the ALS-associated gene TDP-43 leads to neuronal death and degeneration in mice. J Clin Invest 2011; 121: 726–38.

Kabashi E, Lin L, Tradewell ML, Dion PA, Bercier V, Bourgouin P, et al. Gain and loss of function of ALS-related mutations of TARDBP (TDP-43) cause motor deficits in vivo. Hum Mol Genet 2010; 19: 671–83.

Kabashi E, Valdmanis PN, Dion P, Spiegelman D, McConkey BJ, Vande Velde C, et al. TARDBP mutations in individuals with sporadic and familial amyotrophic lateral sclerosis. Nat Genet 2008; 40: 572–4.

Körner S, Kollewe K, Fahlbusch M, Zapf A, Dengler R, Krampfl K, et al. Onset and spreading patterns of upper and lower motor neuron symptoms in amyotrophic lateral sclerosis. Muscle Nerve 2011; 43: 636–42.

Li Y, Ray P, Rao EJ, Shi C, Guo W, Chen X, et al. A Drosophila model for TDP-43 proteinopathy. Proc Natl Acad Sci USA 2010; 107: 3169–74.

Mackenzie IRA, Neumann M, Baborie A, Sampathu DM, Plessis DD, Jaros E, et al. A harmonized classification system for FTLD-TDP pathology. Acta Neuropathol 2011; 122: 111–3.

Mishra M, Paunesku T, Woloschak GE, Siddique T, Zhu LJ, Lin S, et al. Gene expression analysis of frontotemporal lobar degeneration of the motor neuron disease type with ubiquitinated inclusions. Acta Neuropathol 2007; 114: 81–94.

Mitsumoto H, Chad DA, Pioro EP. Amyotrophic lateral sclerosis. Philadelphia: F.A. Davis; 1998.

Munoz DG, Greene C, Perl DP, Selkoe DJ. Accumulation of phosphorylated neurofilaments in anterior horn motoneurons of amyotrophic lateral sclerosis patients. J Neuropathol Exp Neurol 1988; 47: 9–18.

Neumann M, Kwong LK, Lee EB, Kremmer E, Flatley A, Xu Y, et al. Phosphorylation of S409/410 of TDP-43 is a consistent feature in all sporadic and familial forms of TDP-43 proteinopathies. Acta Neuropathol 2009; 117: 137–49.

Neumann M, Sampathu DM, Kwong LK, Truax AC, Micsenyi MC, Chou TT, et al. Ubiquitinated TDP-43 in frontotemporal lobar degeneration and amyotrophic lateral sclerosis. Science 2006; 314: 130–3.

Okamoto K, Hirai S, Amari M, Watanabe M, Sakurai A. Bunina bodies in amyotrophic lateral sclerosis immunostained with rabbit anti-cystatin C serum. Neurosci Lett 1993; 162: 125–8.

Ou SH, Wu F, Harrich D, Garcia-Martinez LF, Gaynor RB. Cloning and characterization of a novel cellular protein, TDP-43, that binds to human immunodeficiency virus type 1 TAR DNA sequence motifs. J Virol 1995; 69: 3584–96.

Piao YS, Wakabayashi K, Kakita A, Yamada M, Hayashi S, Morita T, et al. Neuropathology with clinical correlations of sporadic amyotrophic lateral sclerosis:102 autopsy cases examined between 1962 and 2000. Brain Pathol 2003; 13: 10–22.

Polymenidou M, Lagier-Tourenne C, Hutt KR, Huelga SC, Moran J, Liang TY, et al. Long pre-mRNA deletion and RNA missplicing contribute to neuronal vulnerability from loss of TDP-43. Nat Neurosci 2011; 14: 459–68.

Pun S, Santos AF, Saxena S, Xu L, Caroni P. Selective vulnerability and pruning of phasic motoneuron axons in motoneuron disease alleviated by CNTF. Nat Neurosci 2006; 9: 408–19.

Shan X, Chiang PM, Price DL, Wong PC. Altered distributions of gemini of coiled bodies and mitochondria in motor neurons of TDP-43 transgenic mice. Proc Natl Acad Sci USA 2010; 107: 16325–30.

Swarup V, Phaneuf D, Bareil C, Robertson J, Rouleau GA, Kriz J, et al. Pathological hallmarks of amyotrophic lateral sclerosis/frontotemporal lobar degeneration in transgenic mice produced with TDP-43 genomic fragments. Brain 2011; 134: 2610–26.

Tan CF, Eguchi H, Tagawa A, Onodera O, Iwasaki T, Tsujino A, et al. TDP-43 immunoreactivity in neuronal inclusions in familial amyotrophic lateral sclerosis with or without SOD1 gene mutation. Acta Neuropathol 2007; 113: 535–42.

Tateishi T, Hokonohara T, Yamasaki R, Miura S, Kikuchi H, Iwaki A, et al. Multiple system degeneration with basophilic inclusions in Japanese ALS patients with FUS mutation. Acta Neuropathol 2010; 119: 355–64.

Voigt A, Herholz D, Fiesel FC, Kaur K, Müller D, Karsten P, et al. TDP-43-mediated neuron loss in vivo requires RNA-binding activity. PLoS ONE 2010; 5: e12247.

Wils H, Kleinberger G, Janssens J, Pereson S, Joris G, Cuijt I, et al. TDP-43 transgenic mice develop spastic paralysis and neuronal inclusions characteristic of ALS and frontotemporal lobar degeneration. Proc Natl Acad Sci USA 2010; 107: 3858–63.

Xu YF, Gendron TF, Zhang YJ, Lin WL, D'Alton S, Sheng H, et al. Wild-type human TDP-43 expression causes TDP-43 phosphorylation, mitochondrial aggregation, motor deficits, and early mortality in transgenic mice. J Neurosci 2010; 30: 10851–9.

Yokoseki A, Shiga A, Tan CF, Tagawa A, Kaneko H, Koyama A, et al. TDP-43 mutation in familial amyotrophic lateral sclerosis. Ann Neurol 2008; 63: 538–42.

Zhang YJ, Xu YF, Cook C, Gendron TF, Roettges P, Link CD, et al. Aberrant cleavage of TDP-43 enhances aggregation and cellular toxicity. Proc Natl Acad Sci USA 2009; 106: 7607–12.

Journal of General Virology (2012), 93, 594–602 DOI 10.1099/vir.0.038075-0

Geographical, genetic and functional diversity of antiretroviral host factor TRIMCyp in cynomolgus macaque (*Macaca fascicularis*)

Akatsuki Saito,[1]† Ken Kono,[2]† Masako Nomaguchi,[3] Yasuhiro Yasutomi,[4] Akio Adachi,[3] Tatsuo Shioda,[2] Hirofumi Akari[1,4] and Emi E. Nakayama[2]

Correspondence
Hirofumi Akari
akari@pri.kyoto-u.ac.jp
Emi E. Nakayama
emien@biken.osaka-u.ac.jp

[1]Primate Research Institute, Kyoto University, Inuyama 484-8506, Japan

[2]Department of Viral Infections, Research Institute for Microbial Diseases, Osaka University, Suita 565-0871, Japan

[3]Department of Microbiology, Institute of Health Biosciences, The University of Tokushima Graduate School, Tokushima 770-8503, Japan

[4]Tsukuba Primate Research Center, National Institute of Biomedical Innovation, Tsukuba 305-0843, Japan

The antiretroviral factor tripartite motif protein 5 (*TRIM5*) gene-derived isoform (TRIMCyp) has been found in at least three species of Old World monkey: rhesus (*Macaca mulatta*), pig-tailed (*Macaca nemestrina*) and cynomolgus (*Macaca fascicularis*) macaques. Although the frequency of TRIMCyp has been well studied in rhesus and pig-tailed macaques, the frequency and prevalence of TRIMCyp in cynomolgus macaques remain to be definitively elucidated. Here, the geographical and genetic diversity of TRIM5α/TRIMCyp in cynomolgus macaques was studied in comparison with their anti-lentiviral activity. It was found that the frequency of TRIMCyp in a population in the Philippines was significantly higher than those in Indonesian and Malaysian populations. Major and minor haplotypes of cynomolgus macaque TRIMCyp with single nucleotide polymorphisms in the cyclophilin A domain were also found. The functional significance of the polymorphism in TRIMCyp was examined, and it was demonstrated that the major haplotype of TRIMCyp suppressed human immunodeficiency virus type 1 (HIV-1) but not HIV-2, whilst the minor haplotype of TRIMCyp suppressed HIV-2 but not HIV-1. The major haplotype of TRIMCyp did not restrict a monkey-tropic HIV-1 clone, NL-DT5R, which contains a capsid with the simian immunodeficiency virus-derived loop between α-helices 4 and 5 and the entire *vif* gene. These results indicate that polymorphisms of TRIMCyp affect its anti-lentiviral activity. Overall, the results of this study will help our understanding of the genetic background of cynomolgus macaque TRIMCyp, as well as the host factors composing species barriers of primate lentiviruses.

Received 2 October 2011
Accepted 22 November 2011

INTRODUCTION

Human immunodeficiency virus type 1 (HIV-1) barely replicates in Old World monkeys such as cynomolgus macaques (CMs; *Macaca fascicularis*) and rhesus macaques (RMs; *Macaca mulatta*). This species barrier has long hampered the use of Old World monkeys for human immunodeficiency virus type 1 (HIV-1) research. Recently, a number of intrinsic anti-HIV-1 cellular factors, including tripartite motif protein 5α (TRIM5α), cyclophilin A (CypA), the apolipoprotein B mRNA-editing enzyme catalytic polypeptide-like 3 (APOBEC3) family and tetherin were identified in Old World monkey cells (Nomaguchi *et al.*, 2008; Sauter *et al.*, 2010). Of these factors, TRIM5α was found to strongly suppress HIV-1 replication, mainly by affecting the virus disassembly step, resulting in a decrease in reverse-transcription products (Nakayama & Shioda, 2010; Stremlau *et al.*, 2004). TRIM5α contains a RING domain, a B-box domain, a coiled-coil domain and a PRYSPRY (B30.2) domain. Importantly, the PRYSPRY domain recognizes the capsid of incoming retroviruses, leading to post-entry restriction of infection. RM and CM TRIM5α restrict HIV-1 but not simian immunodeficiency virus isolated from an infected rhesus macaque (SIVmac) (Nakayama *et al.*, 2005; Stremlau *et al.*, 2004; Yap *et al.*, 2004). In the case of HIV-2

†These authors contributed equally to this work.

The GenBank/EMBL/DDBJ accession numbers for the sequences of CM TRIMCyp-major (DK) and RM TRIMCyp are AB671588 and AB671589, respectively.

Two supplementary tables are available with the online version of this paper.

infection, viruses carrying proline (P) at aa 120 of the capsid protein are sensitive to CM TRIM5α, whereas those with either alanine or glutamine (Q) are resistant (Song *et al.*, 2007). Both CM TRIM5α-sensitive and -resistant HIV-2 strains are restricted by RM TRIM5α, and three amino acid residues – threonine (T), phenylalanine (F) and P at aa 339, 340 and 341, respectively – of RM TRIM5α are important for restricting particular HIV-2 strains, which are still resistant to CM TRIM5α (Kono *et al.*, 2008). It is also known that TRIM5α exhibits a high degree of sequence variation, even within macaque species. In some individual RMs, the TFP residues at aa 339–341 of TRIM5α are replaced with a single Q (Newman *et al.*, 2006) and this TFP→Q polymorphism affects the anti-lentiviral activity of RM TRIM5α (Kirmaier *et al.*, 2010).

Although pig-tailed macaques (PMs; *Macaca nemestrina*) have long been thought to exhibit a higher susceptibility to HIV-1 infection than RMs and CMs (Agy *et al.*, 1992), the underlying mechanism determining this difference remained unclear. Recently, a TRIM5–CypA chimeric protein, referred to as TRIMCyp, was discovered in PMs, and the monkeys exclusively expressed TRIMCyp but not TRIM5α (Brennan *et al.*, 2008; Liao *et al.*, 2007). TRIMCyp is an alternatively spliced isoform of the *TRIM5* gene in which the PRYSPRY domain of TRIM5α is replaced with a retrotransposed *CypA* gene. The retrotransposition of the *CypA* sequence in the 3′ UTR of the *TRIM5* gene correlates with a single nucleotide polymorphism (SNP) at the exon 7 splice-acceptor site, leading to skipping of exons 7 and 8 encoding the PRYSPRY domain and splicing to the *CypA* insertion. Thus, the presence or absence of the *CypA* sequence in the 3′ UTR results in expression of TRIMCyp or TRIM5α, respectively.

In vitro analyses demonstrated that cells expressing PM TRIMCyp restricted HIV-2 but not HIV-1 infection (Brennan *et al.*, 2008; Liao *et al.*, 2007), suggesting that the characteristic isoform of the *TRIM5* gene in PMs may be one of the reasons for their greater susceptibility to HIV-1 infection. Furthermore, TRIMCyp was also identified in some individual RMs and CMs (Brennan *et al.*, 2008; Newman *et al.*, 2008; Wilson *et al.*, 2008a). RM TRIMCyp, as well as that of PMs, is unable to restrict HIV-1 infection (Wilson *et al.*, 2008a). This report also showed that the frequency of TRIMCyp in Indian RMs was approximately 25 %, whilst it was not found in the Chinese RM population, suggesting a geographical deviation in the frequency of TRIMCyp (Wilson *et al.*, 2008a). In the case of CMs, although the existence of TRIMCyp has been reported (Brennan *et al.*, 2008), the allele frequency, geographical distribution and relevance in antiviral activity of TRIMCyp remain to be elucidated. As the *TRIM5* gene-related factors are expected to have an impact on the replication of retroviruses, information about the genetic background of CM TRIMCyp will contribute to our understanding of host factors composing the species barrier. In the present study, we studied the geographical, genetic and functional diversity of CM TRIMCyp originating from South-West Asia (Indonesia, Malaysia and the Philippines). We showed a geographical deviation in the frequency of TRIMCyp. Moreover, we found SNPs in CM TRIMCyp and analysed their impact on the anti-lentiviral functions, including their effect against HIV-1, HIV-2, SIVmac and monkey-tropic HIV-1 (HIV-1mt).

RESULTS

Geographical deviation in the frequency of CM TRIMCyp

Initially, we analysed the frequencies of TRIM5α and TRIMCyp genotypes in 126 CMs originating from three different regions – Indonesia, Malaysia and the Philippines – using a PCR-based assay designed to differentiate between the presence and absence of the *CypA* insertion (Fig. 1a) (Wilson *et al.*, 2008a). Insertion of the *CypA* gene in TRIMCyp resulted in a PCR product larger than the expected size for TRIM5α (Fig. 1b).

As shown in Table 1, 35 of the 46 Philippine individuals were homozygous for TRIMCyp, ten were heterozygous and only one was homozygous for TRIM5α. In contrast, only three of the 33 Indonesian individuals were homozygous for TRIMCyp, 17 were heterozygous and 13 were homozygous for TRIM5α. Interestingly, the Malaysian population was of intermediate proportions: ten TRIMCyp homozygotes, 26 heterozygotes and 11 TRIM5α homozygotes. As shown in Fig. 2, the percentages of individuals having each *TRIM5* genotype indicated that the frequency of TRIMCyp homozygotes in Malaysian CMs was twice that in Indonesian CMs. In contrast, the frequency of TRIM5α homozygotes in Indonesian CMs was twice that in Malaysian CMs. Taken together, the calculated allele frequencies of TRIMCyp in the Philippine, Indonesian and Malaysian CM populations were 87.0, 34.8 and 48.9 %, respectively (Table 1). Statistical analyses using a χ^2 test followed by Bonferroni correction demonstrated that the frequency of TRIMCyp in the Philippine population was significantly higher than that in the Indonesian ($P<0.0001$) and Malaysian ($P<0.0001$) populations. In contrast, there was no significant difference between the Indonesian and Malaysian populations ($P=0.2295$).

It should be noted that our method failed to distinguish homozygotes from hemizygotes, especially when the subjects exhibited no polymorphisms in the *TRIM5* gene. However, hemizygosity for the *TRIM5* gene is highly unlikely for the following reasons: (i) the *TRIM5* gene is on an autosomal chromosome, (ii) there is no precedent of deletion of the *TRIM5* gene in humans or primates, and (iii) all of the three CM populations in Table 1 are in Hardy–Weinberg equilibrium for *TRIM5* genotypes.

Polymorphisms in the *CypA* domain of CM TRIMCyp

Previously, it was reported that aa 357 of CM TRIMCyp, corresponding to aa 54 counting from the methionine of

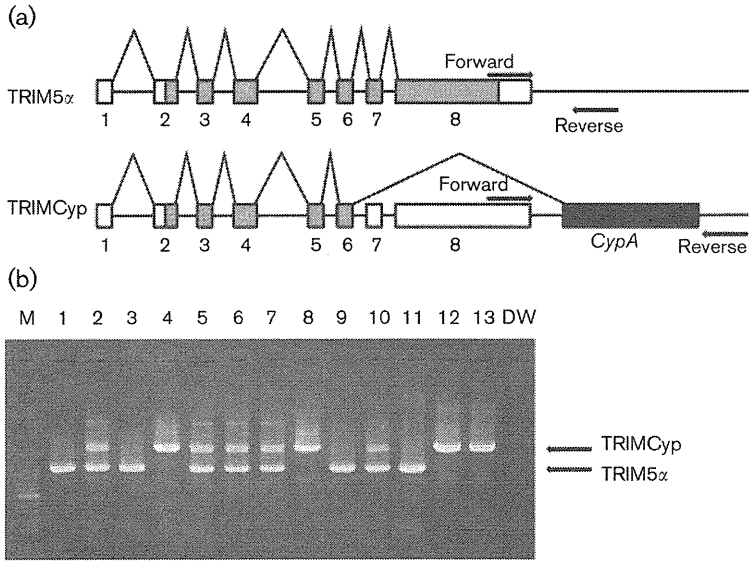

Fig. 1. Determination of *CypA* insertion. (a) Diagram indicating the splicing of TRIM5α or TRIMCyp. Non-coding and coding exons (numbered) and *CypA* sequences are indicated as open, shaded and filled boxes, respectively. The primers used in this study are indicated by arrows. (b) Genomic DNA was extracted from PBMCs. To test for *CypA* insertion, the 3′ region of the *TRIM5* gene was amplified by PCR with primers spanning the 3′ UTR and the putative *CypA* insertion. DW, Distilled water control.

CypA, was arginine (R) (Brennan *et al.*, 2008). Subsequently, Ylinen *et al.* (2010) reported another allele of CM TRIMCyp encoding histidine (H) at this position. To determine the frequency of this R→H polymorphism, we examined 34 TRIM5α/TRIMCyp heterozygotes and 30 TRIMCyp homozygotes for sequence variations in the CypA domain. The results showed that there was no TRIMCyp allele encoding R at position 357 (Cyp 54R). All 94 CM chromosomes carrying the TRIMCyp gene encoded TRIMCyp with H at this position. This result was consistent with the results reported recently by Dietrich *et al.* (2011).

Dietrich *et al.* (2011) also reported CM TRIMCyp polymorphisms at aa 369 and 446, corresponding to aa 66 and 143 in the CypA domain, respectively. Both Brennan *et al.* (2008) and Ylinen *et al.* (2010) reported that aa 369 (Cyp66) and 446 (Cyp143) are aspartic acid (D) and lysine (K), respectively (denoted as the DK haplotype), whilst Dietrich *et al.* (2011) showed the presence of another haplotype encoding asparagine (N) and glutamic acid (E) at positions 369 (Cyp66) and 446 (Cyp143), respectively (denoted as the NE haplotype). Our results showed that 12 CM chromosomes carried TRIMCyp with the NE haplotype, whilst the remaining 82 TRIMCyp were all the DK haplotype (Table 2). Residues 369N (Cyp 66N) and 446E (Cyp 143E) were also found in PM and RM TRIMCyps, and the CypA portion of the NE haplotype of CM TRIMCyp has the same amino acid sequence as RM TRIMCyp (GenBank accession no. EU157763). These results indicate that the previously recognized interspecies variations of the CypA sequence of TRIMCyp were in fact intraspecies variation within CMs. With respect to the geographical distribution of these haplotypes, we found no significant deviation in the frequencies of the haplotypes among the three origins (Table 2).

Polymorphisms in the RING, B-box, coiled-coil, linker and PRYSPRY domains of CM TRIM5α and TRIMCyp

To identify polymorphisms that are in possible linkage disequilibrium with either the DK or NE haplotype in regions other than the CypA domain, we determined nucleotide sequences of TRIM5α and TRIMCyp cDNAs encoding the RING, B-box, coiled-coil and linker domains of six TRIMCyp homozygotes (three homozygotes of the DK haplotype and three heterozygotes for the DK and NE haplotypes) and three TRIM5α homozygotes (see Supplementary Table S1, available in JGV Online). We found polymorphisms at positions 4 [E→glycine (G)] in

Table 1. Frequencies of TRIMCyp alleles in CM populations

Origin	No. of animals	Genotype (no. of animals)			Allele frequency (%)	
		TRIM5α homozygote	TRIM5α/TRIMCyp heterozygote	TRIMCyp homozygote	TRIM5α	TRIMCyp
Philippines	46	1	10	35	13.0	87.0
Malaysia	47	11	26	10	51.1	48.9
Indonesia	33	13	17	3	65.2	34.8

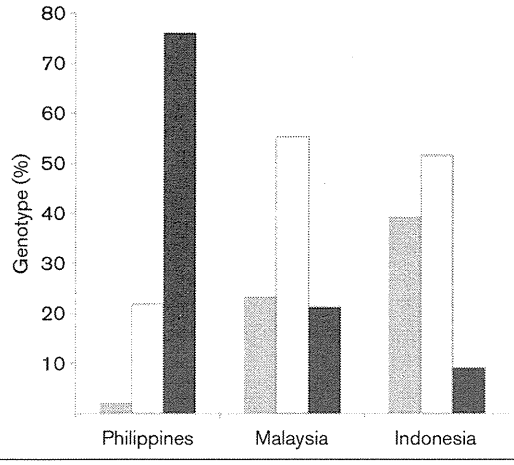

Fig. 2. Frequency of individuals having each *TRIM5* genotype. The percentages of TRIM5α homozygotes and heterozygotes and TRIMCyp homozygotes in each population were calculated. Grey bars, TRIM5α homozygote; white bars, heterozygote; black bars, TRIMCyp homozygote.

the N-terminal region, 44 (K→E) in the RING domain, 178 [H→tyrosine (Y)] and 209 (K→E) in the coiled-coil domain, and 247 (E→D) and 285 (G→R) in the linker domain (Fig. 3a). We found only one chromosome for minor allele 4G, two for 44E, four for 178Y, nine for 209E, five for 247D and four for 285R among 18 chromosomes from the six TRIMCyp homozygotes and three TRIM5α homozygotes. Among the six TRIMCyp homozygotes, we also found three E→Q substitutions at aa 296, which was present in TRIMCyp but absent from TRIM5α. There was no polymorphism that showed strong linkage disequilibrium with either the DK or NE haplotype except for G285R. The NE haplotype tended to link with 285G, although several DK haplotypes also linked with 285G (Supplementary Table S1). The numbers of polymorphic positions were relatively small among CMs compared with RMs (Fig. 3b). It is known that the coiled-coil region of *TRIM5* genes shows a high degree of genetic diversity in RMs (Johnson & Sawyer, 2009). In contrast, the coiled-coil domain of CM TRIM5α and TRIMCyp showed no polymorphism at aa 184, 196, 208, 222, 230 and 236, which were all highly polymorphic in RMs (Newman *et al.*, 2006). These results suggest that the evolutionary pressures targeting the coiled-coil domain of the *TRIM5* gene were weaker in CMs than in RMs.

We also determined the nucleotide sequences of exon 8 encoding the PRYSPRY domain, of 12 TRIM5α homozygotes including the three TRIM5α homozygotes analysed above (see Supplementary Table S2, available in JGV Online). We found polymorphisms at aa 311 [serine (S)→leucine (L)], 327 (P→T), 330 [valine (V)→methionine (M)], 350 [V→isoleucine (I)] and 435 (I→V) in the PRYSPRY domain (Fig. 3a). Among the 12 TRIM5α homozygotes, we did not find a TFP allele at aa 339–341, which is a major determinant for different virus specificity between CM and RM TRIM5αs (Kono *et al.*, 2008) and is also critical for SIV from sooty mangabeys (SIVsm) (Kirmaier *et al.*, 2010) and SIVmac (Lim *et al.*, 2010) restriction by RM TRIM5α. We found only one chromosome for minor allele 311L, one for 327T, one for 350I and four for 435V among 11 TRIM5α homozygotes. We previously cloned CM TRIM5α cDNA from HSC-F cells (GenBank accession no. AB210052) (Nakayama *et al.*, 2005) and found that it contained 330V; however, all of the sequences determined in the present study showed M at this position. In contrast, exon 8 of the TRIMCyp gene of seven TRIMCyp homozygotes (all were heterozygotes for the DK and NE haplotypes), which encoded the PRYSPRY domain but was absent from the mRNA due to splicing, showed a uniform sequence identical to that of the Mamu 7 haplotype of RMs (307P, 313V, 327P, 332R, 333T, 334Q, 339Q, 345I, 383P, 414V, 420S and 488M). We only found one F→L substitution at position 454 among the seven TRIMCyp homozygotes. The Mamu 7 sequence is thus likely to be an ancient prototype sequence of TRIMCyp before the separation of CMs from RMs.

Anti-lentiviral activity of CM TRIMCyps

To elucidate the impact of CM TRIMCyp and its SNPs on the anti-lentiviral activity, we constructed a recombinant

Table 2. Frequencies of DK and NE haplotypes in CM TRIMCyps

Origin	No. of animals	Genotype (no. of chromosomes)				Frequency (%)	
		TRIM5α/TRIMCyp heterozygote*		TRIMCyp homozygote†		DK	NE
		DK	NE	DK	NE		
Philippines	28	6	1	36	6	85.7	14.3
Malaysia	21	14	1	10	2	88.9	11.1
Indonesia	15	12	0	4	2	88.9	11.1

*Haplotypes were determined by direct sequencing of the PCR products.
†Haplotypes were inferred by maximum-likelihood estimation using the results of direct sequencing of the PCR products.

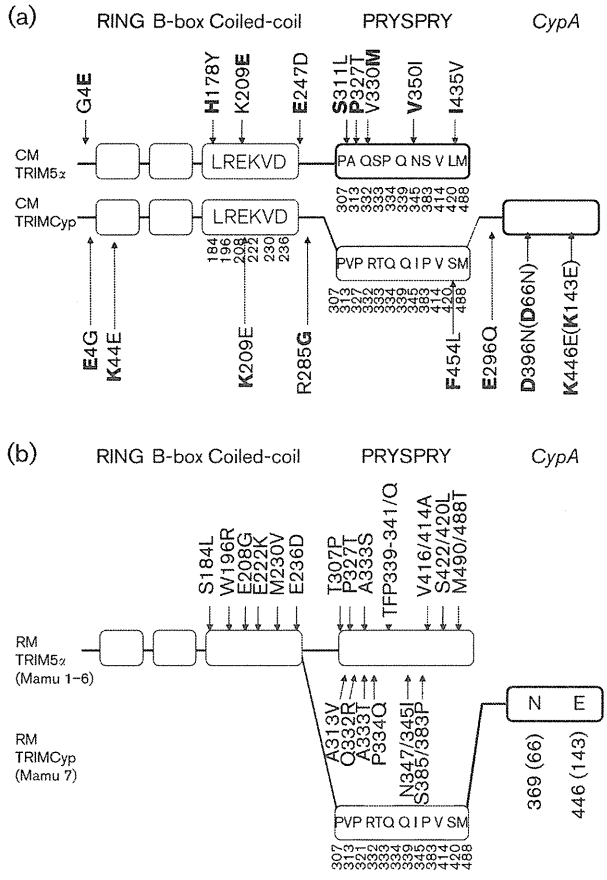

Fig. 3. Sequence variations in TRIM5α and TRIMCyp. (a) Sequence variations in CM TRIM5α and TRIMCyp. The RING, B-box, coiled-coil, PRYSPRY and *CypA* domains of CM TRIM5α and TRIMCyp are indicated by open boxes. The box with thin lines shows exons 7 and 8 of the TRIMCyp gene, which is absent from the mRNA. Polymorphisms are shown outside the boxes, with downward and upward arrows indicating the polymorphisms observed among TRIM5α homozygotes and TRIMCyp homozygotes, respectively. Amino acid residues found in HSC-F cells are shown in front of the amino acid positions, followed by the observed polymorphisms. Major alleles are shown in bold. Numbers in parentheses indicate amino acid positions counting from the initiation methionine codon of the *CypA* ORF. Amino acid residues in the boxes are polymorphic in the RM *TRIM5* gene but lack polymorphism in CM TRIM5α or TRIMCyp. Positions of these amino acid residues are shown below the boxes. (b) Sequence variations of RM TRIM5α (Mamu 1–6) and TRIMCyp (Mamu 7). Downward and upward arrows indicate the polymorphisms observed in TRIM5α and TRIMCyp, respectively. Amino acid residues in boxes indicate those of RM TRIMCyp. Positions of these amino acid residues are shown below the boxes.

Sendai virus (SeV) expressing a series of TRIM5α/TRIMCyp: CM TRIM5α, the DK and NE haplotypes of the CM TRIMCyp [CM TRIMCyp-major (DK) and CM TRIMCyp-minor (NE)], CM SPRY (−) in which the PRYSPRY domain was deleted as a negative control for functional TRIM5α and TRIMCyp, and an RM TRIMCyp. We also constructed a recombinant SeV expressing a CM TRIMCyp-minor (NE) carrying G at position 285 (CM TRIMCyp-minor R285G), as the NE haplotype seemed to be in linkage disequilibrium with G at this position (Supplementary Table S1). As shown in Fig. 4[(a), upper panels], TRIMCyp-major (DK) completely restricted HIV-1 NL4-3, weakly restricted HIV-2 GH123 and failed to restrict SIVmac239. In contrast, TRIMCyp-minor (NE) and TRIMCyp-minor R285G inefficiently restricted HIV-1 NL4-3, barely restricted SIVmac239 and completely restricted HIV-2 GH123. These results indicated that the sequence variations in CM TRIMCyp greatly altered the spectrum of its anti-lentiviral activity. It should be noted that HIV-1 NL4-3 attained slightly higher titres at day 3 in cells expressing TRIMCyp-minor R285G than in those expressing TRIMCyp-minor (NE). The difference was small but reproducible in six independent experiments. This result indicated that aa 285 of TRIMCyp also affected its antiviral activity. In the case of RMs, in which the CypA domain of TRIMCyp has the same amino acid sequence as CM TRIMCyp-minor (NE), RM TRIMCyp showed the same spectrum of anti-lentiviral activity as CM TRIMCyp-minor (NE) (Fig. 4a, lower panels), consistent with previous reports (Price *et al.*, 2009; Wilson *et al.*, 2008a).

Finally, we examined whether HIV-1mt NL-DT5R (Kamada *et al.*, 2006) could evade restriction by CM TRIM5α/TRIMCyp. HIV-1mt possesses core antigen (CA) with the SIVmac239-derived loop between α-helices 4 and 5 (L4/5), which corresponds to a CypA-binding loop of HIV-1, the entire SIVmac239 *vif* gene and two non-synonymous substitutions in the *env* gene (Fig. 4b). As shown in Fig. 4(c), NL-DT5R was restricted by TRIM5α but completely evaded restriction by CM TRIMCyp-major (DK), suggesting that replacement of the CypA-binding loop of HIV-1 CA with the corresponding SIVmac239-derived sequence was sufficient to render HIV-1 resistant to the major haplotype of CM TRIMCyp but not TRIM5α.

DISCUSSION

In the present study, we analysed the geographical, genetic and functional diversity of CM TRIMCyp and found: (i) a clear geographical deviation in the frequency of TRIMCyp, (ii) no typical geographical deviation in the frequency of the DK/NE haplotypes in the CypA domain, and (iii) sequence variations in the CypA domain of CM TRIMCyp, which greatly altered the spectrum of its anti-lentiviral activity.

We first demonstrated that the allele frequency of TRIMCyp in CMs from the Philippines was significantly higher than those in Indonesian and Malaysian CMs. It is possible that some pathogen(s) resistant to the antiviral effect of either TRIM5α or TRIMCyp may contribute to this deviation as a selective pressure. As primate lentiviruses such as HIV-1 and

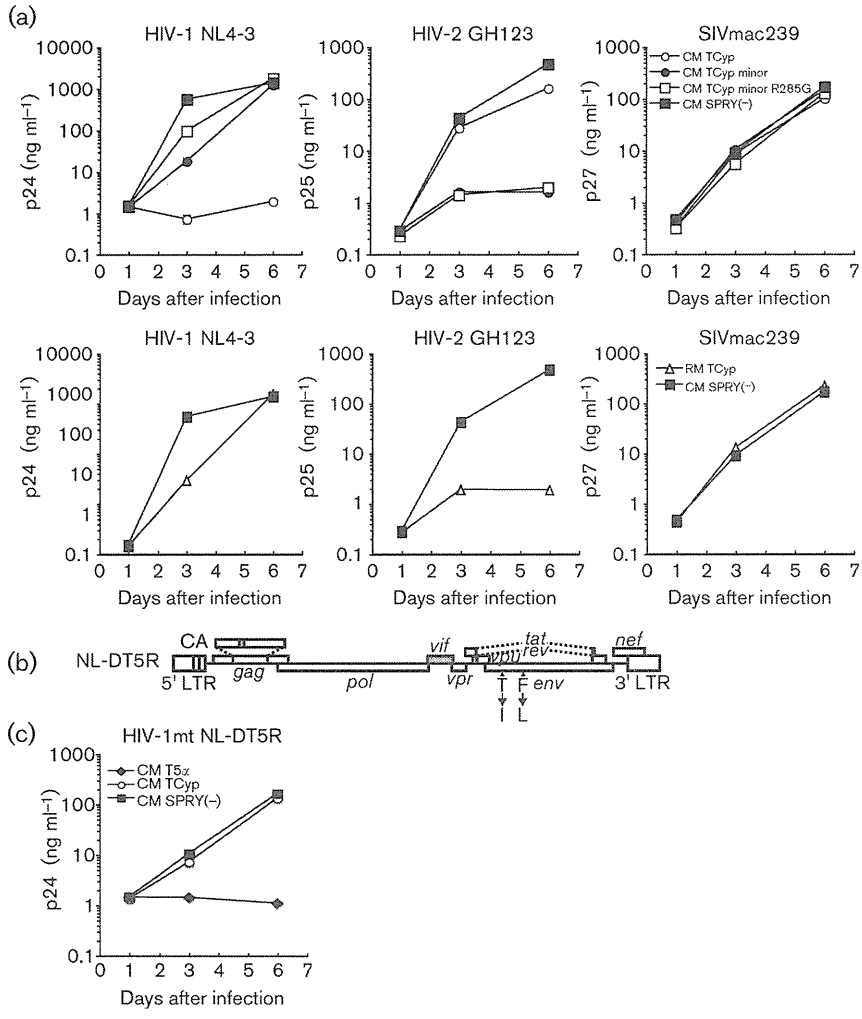

Fig. 4. Anti-lentiviral activity of various CM TRIMCyp. (a) MT4 cells were infected with recombinant SeV expressing CM TRIMCyp-major (DK) (CM TCyp; ○), CM TRIMCyp-minor (NE) (CM TCyp minor; ●), CM TRIMCyp-minor R285G (CM TCyp minor R285G; □), CM SPRY (−) (■) or RM TRIMCyp (RM TCyp; △). Data for CM SPRY (−) in the upper and lower panels were identical. Nine hours after infection, cells were superinfected with HIV-1 NL4-3, HIV-2 GH123 or SIVmac239. Culture supernatants were assayed separately for levels of p24, p25 or p27. (b) Structure of HIV-1mt NL-DT5R used in the experiment shown in Fig. 3(c). Open boxes denote HIV-1 (NL4-3) and shaded boxes denote SIVmac239 sequences. (c) MT4 cells were infected with recombinant SeV expressing CM TRIM5α (CM T5α; ◆), CM TRIMCyp-major (DK) (CM TCyp; ○) or CM SPRY (−) (■). Nine hours after infection, cells were superinfected with HIV-1mt NL-DT5R. Culture supernatants were assayed separately for levels of p24. Error bars show actual fluctuations between duplicate samples. Data from a representative of three (a) or two (c) independent experiments are shown.

SIV originated in African primates, it is unlikely that these viruses could contribute directly to this deviation, and some exogenous and endogenous retroviruses may thus play a critical role in this selection. Alternatively, it is possible that this deviation could come from bottleneck effects. It is estimated that the Philippine CMs were derived from Indonesian CM stocks via sea rafting or terrestrial access through Borneo during periods of low sea level in South-East Asia around 110 000 years ago (Abegg & Thierry, 2002; Blancher *et al.*, 2008; Kita *et al.*, 2009). Furthermore, phylogenetic analyses of mitochondrial DNA sequences of four CM populations distributed in South-East Asia suggested that Philippine CMs were derived from the small founding populations of Indonesian CMs, resulting in low genetic and nucleotide diversities (Blancher *et al.*, 2008). Importantly, however, as the Philippine CMs involved in this study at least originated from Luzon and Mindanao, the results in this study may reflect the frequency of TRIMCyp